

Scuola di Ingegneria e Architettura  
Corso di Laurea Magistrale in Ingegneria Meccanica

**TESI DI LAUREA MAGISTRALE**  
in  
**Meccanica dei Robot M**

**STUDY OF A NOVEL SOLUTION  
TO OBTAIN CONTROLLABLE STIFFNESS  
FOR BEAM-LIKE ELEMENTS**

Candidato:  
**Giovanni Melandri**

Relatore:  
**Vincenzo Parenti Castelli**

Correlatori:  
**Stefano Stramigioli**  
**Alexander Dijkshoorn**  
**Rocco Vertechy**  
**Nicola Sancisi**



# Abstract

La presente tesi tratta dello studio di concetti volti all'ottenimento di strutture meccaniche a rigidità variabile per applicazioni in ambito di ricerca scientifica, in particolare per una futura applicazione in un robot aereo ad ala battente, al fine di studiare l'interazione tra ala elastica ed aria. Vengono riassunti i metodi per ottenere rigidità variabile ed, in seguito ad una fase di confronto basato su requisiti ed obiettivi di progetto, vengono scelte due soluzioni. Il lavoro mostra che il concetto "sliding segments" funziona bene per una trave composta da un'asta interna ed un tubo esterno, entrambi formati da segmenti rigidi e flessibili alternati, di due materiali differenti. La rigidità flessionale della trave varia grazie ad una traslazione dell'asta interna. Viene inoltre mostrato come un'asta ed un tubo possono essere combinati per ottenere una trave rotante con diversi livelli di rigidità flessionale in una direzione, riducendo gli effetti della flessione deviata.

The present thesis studies concepts aimed at obtaining mechanical structures with variable stiffness for scientific research purposes, in particular for a future application in a robotic bird, to study wing-air interaction. Variable stiffness mechanisms are reviewed and, after a comparison phase, based on project requirements and objectives, two concepts are chosen. The work shows that the sliding segments concept works well for a spar composed of an inner rod and an outer tube, both formed by rigid and compliant segments made of two different materials. The flexural stiffness of the beam changes by means of translating the inner rod. The thesis also shows how a rod and a tube can be combined to form a rotary spar with multiple flexural stiffness levels in one direction, reducing the effects of deviated bending.



# Contents

<b>1</b>	<b>Introduction</b>	<b>1</b>
<b>2</b>	<b>Variable stiffness solutions review</b>	<b>4</b>
2.1	Geometrical Properties . . . . .	6
2.2	Elastic properties . . . . .	10
2.3	Actuator-like solutions . . . . .	26
2.4	Hybrid . . . . .	31
<b>3</b>	<b>Solutions comparison</b>	<b>33</b>
3.1	Requirements-based comparison . . . . .	33
3.2	Objectives-based comparison . . . . .	36
<b>4</b>	<b>Modelling and Design</b>	<b>40</b>
4.1	Sliding segments . . . . .	40
4.2	Rotary spar . . . . .	51
<b>5</b>	<b>Methodology</b>	<b>56</b>
5.1	Specimens fabrication . . . . .	56
5.2	Experimental set-up . . . . .	62
<b>6</b>	<b>Results &amp; Discussion</b>	<b>66</b>
6.1	Sliding segments . . . . .	66
6.2	Rotary spar . . . . .	76
<b>7</b>	<b>Conclusions and future work</b>	<b>82</b>

# List of Figures

1.1	Robird flying robot, from <a href="https://www.ram.eemcs.utwente.nl">https://www.ram.eemcs.utwente.nl</a> . . .	3
2.1	Origami structure concept, from [7] . . . . .	7
2.2	Tri-stable structure, from [10] . . . . .	8
2.3	Multi-layer beam, thermal activation, from [11] . . . . .	10
2.4	Multi-layer beam, electrostatic activation (EBL), from [12] . . . . .	10
2.5	Piezoelectric flapping wing mechanism, from [14] . . . . .	12
2.6	Frequency-based turn mechanism, from [14] . . . . .	12
2.7	Articulated joint using wax, from [16] . . . . .	13
2.8	Solder-based mechanism in a tunable stiffness spine-like configuration, from [17] . . . . .	14
2.9	Morphing wing concept using SMA wire bundles, from [19] . . . . .	16
2.10	Variable stiffness SMP-based joint, from [21] . . . . .	16
2.11	EAP actuator design: view from above, rest state, activated state, from [22] . . . . .	17
2.12	Soft fluidic continuum arm: flexibility control through ER fluid flow, from [23] . . . . .	18
2.13	Variable stiffness spring using magnetostrictive material, from [24] . . . . .	19
2.14	Granular jamming robotic gripper, working principle, from [26] . . . . .	21
2.15	ELJ beam composition, from [29] . . . . .	22
2.16	Wire jamming (a) vs layer jamming (b), from [3] . . . . .	23
2.17	Segments locking concept using wires, bellows, soft layers, from [3] . . . . .	24
2.18	Snake-like robot concept by using wires segments locking, from [31] . . . . .	25
2.19	Sliding layer concept, from [34] . . . . .	25
2.20	Pneumatic robot link with plastic and silicone chamber, from [36] . . . . .	26
2.21	FFMC: pressure is shared between tubes and matrix, from [38] . . . . .	27

2.22	vsaUT-II: variable lever arm length concept, from [39]	28
2.23	Moving wing spars to obtain an adaptive airfoil, from [40]	29
2.24	Antagonistic approach: antagonistic motors, from [41]	30
2.25	Antagonistic approach: independent motors, from [41]	30
2.26	Variable stiffness carbon nanotube spring-like nanocomposite yarn for artificial muscles, from [42]	31
2.27	Hybrid solution: mechanical translation and layer jamming, from [43]	32
4.1	Acrobat SUV Vacuum Stabilizer: provides local stabilization of a target vessel during off-pump coronary artery bypass, from <a href="http://www.getinge.com">www.getinge.com</a>	41
4.2	Images of sliding segments sample: (a) outer tube, (b) inner rod, (c) compliant unshifted configuration and (d) rigid fully shifted configuration	43
4.3	Sliding segments concept	44
4.4	Small deformed beam angles hypothesis	45
4.5	Possible simplified sections in sliding segments model	48
4.6	Locations of listed sections of fig. 4.5 in sliding segments sample	49
4.7	Elastic lines derived by solving analytic beam model: fully shifted configuration in blue, unshifted configuration in red	51
4.8	Rectangular section rotation	52
4.9	Example of bending along a non principal inertia axis	53
4.10	Example of $\alpha$ reduction due to additional material	55
5.1	Geometrical parameters describing the built samples	57
5.2	Onyx sample: inner and outer parts, unshifted configuration, fully shifted configuration	58
5.3	Aluminium sample manufacturing	59
5.4	Aluminium sample: inner and outer parts, unshifted configuration, fully shifted configuration	60
5.5	Multi-material sample: inner and outer parts, unshifted configura- tion, fully shifted configuration	61
5.6	SMAC LCA25-050-15F linear actuator used for bending tests	63
5.7	Scheme of the built set-up to perform bending tests for beam elements	64

5.8	Experimental set-up to derive flexural stiffness of beam-like elements subjected to bending . . . . .	64
5.9	Examples of measured displacement, measured force, force-displacement curves with error analysis, relative to multi-material sample bending test . . . . .	65
6.1	Bending tests results for Onyx prototype as sliding segments beam	67
6.2	Bending tests results for Aluminium prototype as sliding segments beam . . . . .	69
6.3	Bending tests results for multi-material prototype as sliding segments beam . . . . .	71
6.4	Multi-material prototype: stiffness-shifting curves . . . . .	71
6.5	Simulations of sliding layer concept, with different stiffness of rigid parts: $ErIr$ and $EsIs$ are flexural stiffness of rigid and soft layers, $n$ is their ratio, $K_{effec}$ is global stiffness and $L$ length of the laminate. From [34] . . . . .	74
6.6	Example of not overlapped bended parts, from [34] . . . . .	75
6.7	Multi-material prototype: stiffness-shifting mean curve . . . . .	76
6.8	Multi-material prototype: stiffness-overlapping mean curve . . . . .	76
6.9	Bending tests results for Onyx rod as rotary spar . . . . .	78
6.10	Onyx rotary rod: stiffness-angle curves . . . . .	79
6.11	Bending tests results for Onyx prototype as rotary spar . . . . .	80
6.12	Onyx rotary spar, rod + tube: stiffness-angle curves . . . . .	81
7.1	Example of alternative configurations achievable by changing flexures spatial frequency . . . . .	84
7.2	Possible integration of sliding segments and rotary spar . . . . .	85

# List of Tables

2.1	Variable stiffness solutions, with a classification based on [3] . . . .	5
3.1	Requirements-based comparison. “Y” and “N” represent “satisfied” and “not satisfied”, respectively. . . . .	35
3.2	Objectives ranking . . . . .	38
3.3	Objective-based comparison . . . . .	38
5.1	Geometrical properties for Onyx prototype . . . . .	57
5.2	Geometrical properties for aluminium prototype . . . . .	59
5.3	Geometrical properties for multi-material prototype . . . . .	61

# Chapter 1

## Introduction

Robird is a robotic bird of prey presented in 2016 by University of Twente [1] (fig. 1.1). It is a system that mimics the behaviour of its biological counterpart, with many brilliant features: for instance, it can stably fly up to 80 km/h, in different wind conditions [2]. It was developed at RAM, Robotics and Mechatronics research group.

The actual Robird cannot take off on its own, cannot perch, uses symmetric flapping, steers using a number of manifolds placed in the tail and has a minimal autonomy and a restricted operation time due to power consumption.

Portwings is a European Research Council funded project, officially started in 2018, aimed at understanding the physics of flapping flight to the scientific depth needed to go even further in the robotics field.

Through Portwings a much deeper structured understanding of flapping flight will be gained, and these understandings will be experimentally validated. This will be done using port-Hamiltonian system theory and its physically unifying character, which will couple fluid dynamics theory to dynamically changing surfaces and their actuation [2].

One of the areas of focus for the research is aerodynamics, especially wing-air interaction. Furthermore, it is of scientific interest to study the effects of wing flexibility on flapping flight aerodynamics.

In aeroelasticity studies about flapping flight papers prevail based on experimental analyses, revealing the importance of the elastic behaviour of birds' wings.

In fact, the lack of mathematical models able to explain and predict this kind of phenomena depicts one of the gaps which the Portwings project aims to fill, hand in hand with experimental studies.

Anyway, the flexural and torsional deformations of a wing contribute to determine fundamental characteristics of the wing-air interface, such as the angle of attack. Therefore wing stiffness control of course represents an important additional control parameter.

Hence comes the idea to implement the possibility to vary the stiffness of a wing, which is an existent topic in literature (e.g. [11], [12], [19], [40]). Stiffness variations can allow to study, through wind tunnel tests, the aerodynamics of wings with various flexibility characteristics. Moreover, with this type of solution it could be possible to search for advantages of a wing that can change its stiffness during flight.

This study wants to move some steps towards the goal of building a flying robot able to achieve controlled wing deflections during flight, which maximize in every instant aerodynamic parameters such as lift and thrust, reducing the power consumption.

In particular, the present thesis, as a first work in this direction, aims to answer the following research question: “what are the best concepts and techniques targeted to implement variable stiffness in a flapping wing, especially as part of a smart wing spar?”

The general approach is based on an initial study of the state of the art. The work then converges to a detailed analysis of solutions considered to be more adequate to design a smart spar with controllable rigidity.

Methodology comprises the development of a first try mathematical model of variable stiffness beams, the manufacturing of different kinds of specimens and the preparation of an experimental set-up to perform bending tests.

Results are analysed and discussed, including recommendations for future works.



Figure 1.1: Robird flying robot, from <https://www.ram.eemcs.utwente.nl>

# Chapter 2

## Variable stiffness solutions review

In this chapter most solutions to obtain variable stiffness elements in robotics are summarized. Examples are shown for each described concept. The objective of this chapter is to give an overview of the existing solutions and methods to be compared for the purpose of this work.

As far as the author knowledge goes, nobody has tried to combine active stiffness control and flapping wing aerodynamics yet. Nevertheless, there are many technologies, especially applied in soft robotics, medicine and fixed wings aerodynamics fields, that could be of inspiration for a new concept of flexible flapping wing.

Flexural and torsional stiffness of a structure considers both intrinsic material properties and geometry of the structure itself. Two families of variable stiffness solutions are defined by concepts for which these two characteristics are modified. Another family might be represented by the actuator-like solutions, resisting the bending forces applied to the structure. This classification is presented by L. Blanc et al., who propose a useful overview of the controllable stiffness mechanisms and solutions for medical devices [3]. Such scheme is taken as a starting point to classify the main technologies, together with other review articles, e.g. [4], [5], [6]. Variable stiffness solutions that will follow are summarized in table 2.1.

The author wants to highlight that, for this project purposes, concepts based on distributed systems are of more interest, due to the final goal outlined in the previous chapter. Some of described solutions, though, are about variable stiffness joints or other systems featured by one single degree of freedom, which can be considered as a different topic. These concepts are inserted for the sake of completeness and especially because of the useful insights their working principles can provide.

Geometrical properties	Cross section shaping	Origami structures Pneumatic expansion Multi-stable structures
	Structural interactions	Multi-layer beams
Elastic properties	Material	Piezoelectric materials Low melting point materials Wax Solder Shape memory materials Electroactive polymers Rheological fluids Magnetostrictive materials Electrostrictive materials Biomaterials
	Structural interactions	Granular jamming Turgor pressure Layer jamming Wire jamming Segments locking
Actuator-like solutions	Fluid-based solutions	Pneumatic Hydraulic Fluidic Flexible Matrix Composites
	Mechanical solutions	Component translation/rotation Antagonistic approach Muscles

Table 2.1: Variable stiffness solutions, with a classification based on [3]

## 2.1 Geometrical Properties

A stiffness variation can be obtained either by modifying the cross-section or, in case of heterogeneous structure, by changing the structural interactions of the elements forming the geometry.

### 2.1.1 Cross section shaping

Changing the cross section leads to a direct change in the second moment of area of the structure, without varying the material properties.

#### Origami structures

They are structures that show a changeable geometry through folding operations. Due to geometrical change, different flexural behaviours are obtained in the folded/unfolded state.

S. Mintchev et al. managed to build an origami structure inspired from dragonfly wings. It's made of a prestretch elastomer membrane between two rigid tiles [7]. The tiles don't cover the membrane where the origami must fold. The structure displays high stiffness for axial loads below a threshold, then softens when the threshold is exceeded (dual stiffness behaviour due to the changeable geometry). For the same reasons the origami only folds when the threshold is exceeded. It shows a load bearing behaviour in the stiff state, resilience and safe interaction with objects in the soft state. Moreover, the membrane stores elastic energy during folding (fig. 2.1). This technology has been used to build crash resilient blades for a quadcopter and a compliant gripper, but it could be applied to the field of morphing wing structures as well.

Another interesting solution is described in [8], where a tendon driven origami structural element is used to build a variable stiffness wrist brace.

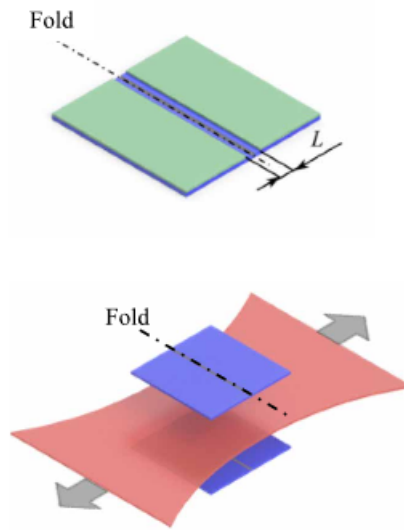


Figure 2.1: Origami structure concept, from [7]

### **Pneumatic expansion**

This technology just relies on a flexible hollow structure that can vary its stiffness properties thanks to a pressure distribution generated by a pneumatic system. In other words, inflatable elements show stiffness variations due to changes in their dimension. It has to be noted that in this case the goal is to change the geometry, without resistance to the expansion, while in other solutions that will follow the stiffness change will be thanks to a pressure difference without substantial geometric variations.

To give an example, pneumatic expansion concept has been used for deployable wings [9].

### **Multi-stable structures**

A multi-stable structure is a type of composite structure that exhibits multiple stable static configurations. Different stable shapes correspond to different stiffness behaviours. A multi-stable structure settles at one of its equilibrium positions without demanding continuous power to remain there.

If the structure is triggered to leave an equilibrium position, it will snap or jump to the other equilibrium position.

For instance, F. Dai et al. developed a multi-stable lattice structure consisting of a tri-stable lattice cell which is made of bi-stable laminates (fig. 2.2) [10].  $N$  tri-stable lattice cells can exhibit  $2^N$  stable states, and the critical loads between states are obtained numerically.

Also buckling systems can be classified as multi-stable structures: for example, two coil springs pushed one against each other behave differently depending on the angle between them. In particular, the coaxial (unstable) configuration is really compliant, and a small force is sufficient to jump to another equilibrium state.

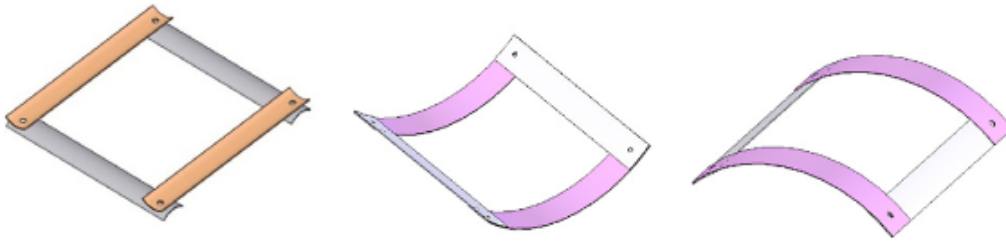


Figure 2.2: Tri-stable structure, from [10]

### 2.1.2 Structural interactions

Structural interactions based solutions can modify their geometrical properties with no macroscopic change in external dimensions, thanks to interactions between elements composing the structure. Here structures are considered as heterogeneous.

#### Multi-layer beams

In the flexible state, beam layers are decoupled, and the global second moment of area corresponds to the sum of single layers' ones. In the rigid state, the layers are coupled, and the structure behaves as a single larger beam with a strongly larger second moment of area. Locking of structural elements can

be obtained by applying a force [12] or by modifying the inter-layers shear properties (e.g. by heating [11]). It should be noted that variations in the second moment of area of the section affect both torsional and flexural beams behaviour.

These structures are classified within two main families:

- Single material multi-layer beams: the heterogeneous structure is composed by different layers made of the same material. The second moment of area is modified by adapting the interactions between layers surfaces.
- Multiple material multi-layer beams: the heterogeneous structure is composed by different layers made of multiple materials. The mechanical properties of some layers are modified in this case. Usually some soft layers (polymeric) are interposed between stiffer ones (typically metallic). The global structural behaviour is modified for instance by heating the polymer [3]. Layers are so decoupled and beam stiffness decreases.

W. Raither et al. proposed a morphing wing concept with controllable twist using “smart spars” [11]. The wing spars were made by a U shaped section aluminium beams combined with a rectangular section multi-layer beam. The layers, from the inner to the outer, were made of PVC, elastomer, and CFRP (Carbon Fiber Reinforced Polymer), respectively. It is a semi-passive system: when PVC is electrically heated, global spar stiffness decreases, allowing aerodynamic loads to twist the wing and improve the aerodynamic performance (fig. 2.3).

W. Raither et al. also proposed a different multi-layer beam with the same purpose. The working principle is no more electrical heating, but electrostatic force [12]. Such composite materials are called Electro Bonded Laminates (EBL): a dielectric layer is interposed between two electrodes of different potential attracting each other. Without current layers are decoupled and the structure is compliant, then when current flows layers become coupled and shear forces can be transmitted by friction at electrode-dielectric interface (fig. 2.4). By activating one of the two smart wing spars one can control the twist of the wing, under certain conditions.

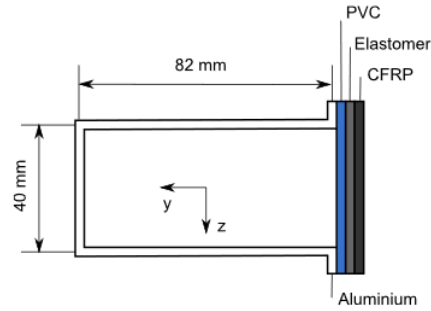


Figure 2.3: Multi-layer beam, thermal activation, from [11]

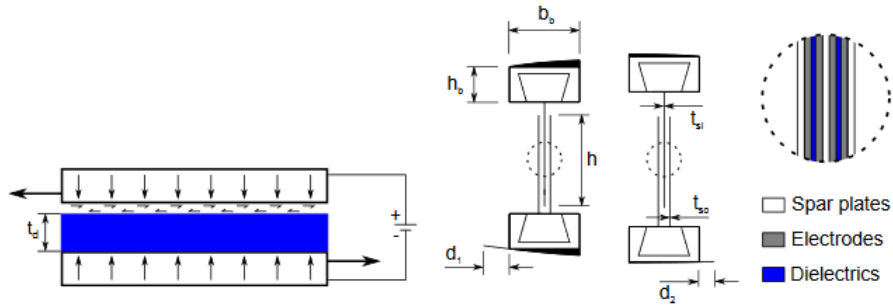


Figure 2.4: Multi-layer beam, electrostatic activation (EBL), from [12]

## 2.2 Elastic properties

Elastic properties of the material can also be varied to obtain different stiffness. In case of a heterogeneous structure, it can be thought as made by an equivalent homogeneous material with same size, because of the generally smaller dimensions of the elements composing it. These equivalent elastic properties can be varied by directly changing material properties of the parts/layers composing the solution or by modifying the interactions between them. It is possible to combine these principles to obtain hybrid solutions.

### 2.2.1 Material

Stiffness variation can be due to intrinsic material properties, and can occur thanks to different phenomena, such as the following ones:

- Piezoelectricity
- Phase transition
- Glass transition
- Electroactive polymers
- Rheological fluids

#### **Piezoelectric materials**

Piezoelectricity is the electric charge that accumulates in certain materials in response to applied mechanical stress. The piezoelectric effect is reversible: these materials can be used as actuators, or sensors. When activated, the internal crystalline structure of piezoelectric materials is deformed. The deformation order of magnitude is really small, so such mechanisms usually need some amplification systems. Some applications include vibration control and sensing. A change in the electrical boundary condition of piezoelectric materials from short circuit (electrically free condition) to open circuit (electrically blocked condition) results in an increase in the Young's modulus. R. Vos and R. De Breuker proposed a morphing wing model with a piezoelectric flight control mechanism for a UAV (Unmanned Air Vehicle) [13]. The mechanism relies on axial precompression to magnify deflections and forces simultaneously, achieving a trailing edge deflection of  $\pm 3^\circ$ , enhancing UAV roll control.

A. Cox et al. developed a mesoscale piezoelectrically actuated flapping wing MAV, inspired by dragonflies [14]. Piezoelectric actuation can be used only to emulate mesoscale flapping flight, because of the short wing stroke length. Simple parallel mechanisms are used with carbon fiber bars (fig. 2.5). The

frequency of command signal is shifted to turn the MAV: for instance, lowering the frequency of left wing would increase its stroke amplitude, which lead to more lift and to a right turn (fig. 2.6). There is a single active degree of freedom: the torsional motion of the wing will be obtained passively through dynamic behaviour.

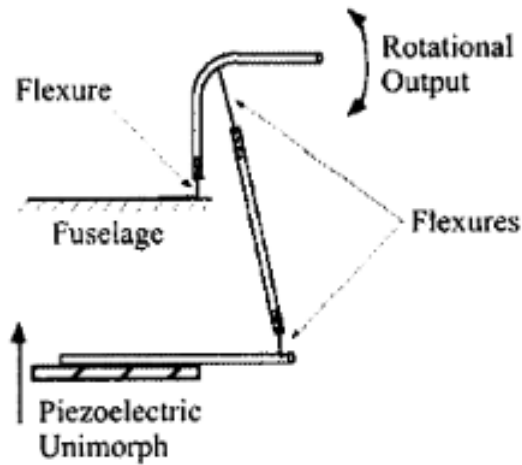


Figure 2.5: Piezoelectric flapping wing mechanism, from [14]

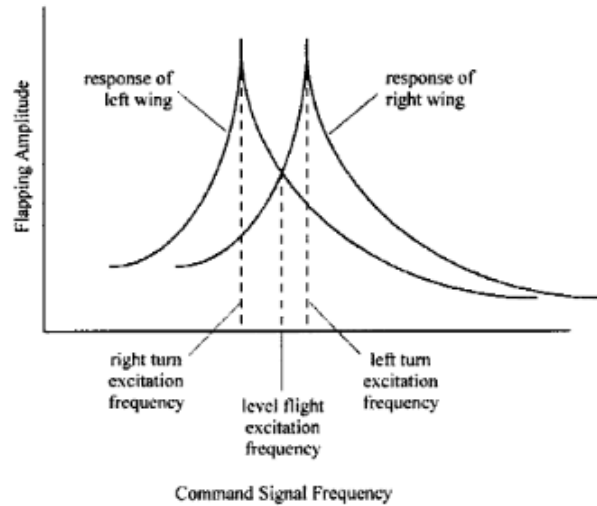


Figure 2.6: Frequency-based turn mechanism, from [14]

## Low melting point materials

These materials drop their stiffness via phase change at not so high temperatures, so the heating mechanisms can be Joule heating by voltage difference, but also hot water, for example. They can be LMPAs (Low Melting Point Alloy) or polymers, with various transition temperatures.

For instance, M. McEvoy and N. Correll presented a tunable stiffness mechanism based on PCL (Polycaprolactone) [15]. Stiffness changes are locally inducted by heating through Nichrome wires. The material becomes rapidly softer after reaching 50°C. In this case a simple on-off controller is sufficient to reach and hold a desired temperature as fast as possible.

## Wax

Structures made of soft material (e.g. foam) covered by stiffer wax. When wax is heated it changes phase and the whole structure assumes the inner material stiffness. This solution is quite available, low-cost and easy to manufacture.

N. Cheng et al. used wax to build an articulated variable stiffness joint, in the field of soft robotics [16]. In figure 2.7 soft and rigid states of the same beam are showed.

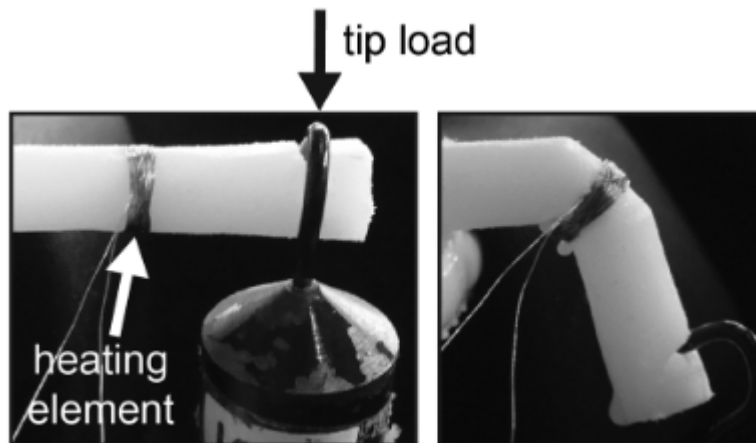


Figure 2.7: Articulated joint using wax, from [16]

## Solder

A controllable stiffness mechanism through solder joints has been applied to crawling robots, based on phase changes within the joints.

N. Cheng et al. proposed an inchworm-like mobile robot that consists of multiple, independent, thermally activated joints, but it's driven by a single actuator [17]. To realize control of this under-actuated system, a solder-based locking mechanism has been developed to selectively activate individual joints without requiring additional actuators (fig. 2.8).

Another example might be represented by silicone spheres with a gallium core which can be melted by using nickel-chromium (nichrome) wires [18].

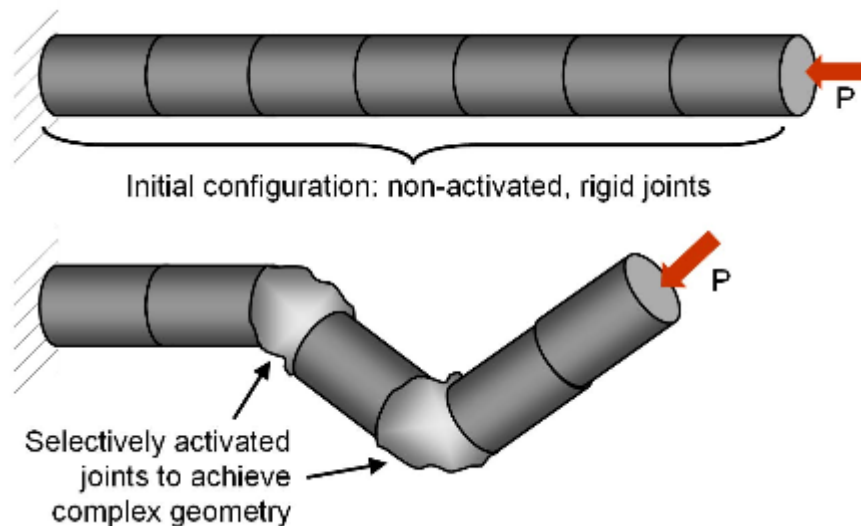


Figure 2.8: Solder-based mechanism in a tunable stiffness spine-like configuration, from [17]

## Shape memory materials

These smart materials can be shape memory alloys (SMA), shape memory polymers (SMP), gels and composites. They can change their shape or properties for a given stimulus and could be used as actuators either for their stiffness change ability.

SMAs are metals that can stay in a desired shape, but they morph to an original different shape via heat stimulus, becoming also stiffer. It is a rapid

variation due to a microstructural change. SMPs are in general more deformable, with a wider elastic modulus range around transition, and lower in cost with respect to shape memory alloys.

The restoring force of SMA as actuating material is impacted by temperature, stress condition and martensite content (type of metal crystal structure). The latter is hard to be detected, so fine control is not easy to be acquired.

C. Bil et al. have developed a morphing wing structure using SMA wire bundles, which work better than single wires because of the improved heat transfer [19]. Bundles also have to be separated to allow the cooling air to flow. The bundles are connected mechanically in parallel and electrically in series in the chordwise direction, in order to obtain a variable camber airfoil (fig. 2.9).

Y. Dong et al. proposed to use SMA springs as actuators, with so much larger travel length than normal wires, to obtain a morphing aircraft wing [20]. SMA springs are similar to basic coil springs, but the shearing module is not constant in time. From external and material data one can derive diameter and number of circles required for the application. Springs have to be electrically isolated and connected in series to obtain the same current, allowing deformation continuity.

L. Hines et al. used a composite SMP structure for hinge stiffness control in a miniature flapping wing robot [21]. When heated, the joint allows also translational motion between the two links, resulting in loss of flapping amplitude and thus loss of lift. While transitioning, change in lift is almost linear with temperature, with little hysteresis. This experimental result demonstrates that any lift value between the fully cooled or heated state could be maintained with close loop temperature control (fig. 2.10).

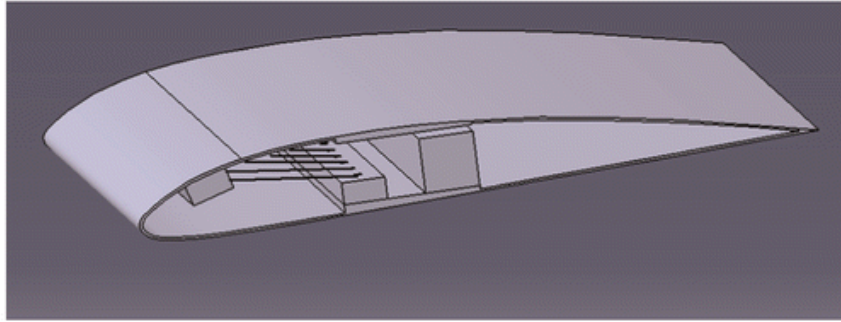


Figure 2.9: Morphing wing concept using SMA wire bundles, from [19]



Figure 2.10: Variable stiffness SMP-based joint, from [21]

### Electroactive polymers

Electroactive polymers (EAPs) are polymers that exhibit a change in size or shape when stimulated by an electric field. The most common applications of these materials are as actuators and sensors. A typical characteristic property of EAPs is that they will undergo a large amount of deformation while sustaining large forces. EAPs have been described as “artificial muscles” due to several muscle-like properties, such as inherent passive compliance and damping, low weight, flexible geometry, and silent operation. However, their disadvantages include high voltage requirements, low bandwidth due to hysteretic losses and actuator failure due to manufacturing defects, mechanical film overstrain and tearing, dielectric breakdown and shorting. Both variable stiffness and damping properties have been demonstrated.

Dielectric elastomers (DE) are a variety of electroactive polymers that deform due to the electrostatic interaction between two electrodes with opposite electric charge.

Another type of EAP are ionic gels (IGLs). Application of voltage causes movement of hydrogen ions in or out of the gel, thus changing the environment from acid to alkaline, causing the gel to become dense or swollen accordingly.

S. Dastoor and M. Cutkosky introduced an EAP variable stiffness device that utilizes the applied voltage (from 0 to 6 kV at 100  $\mu\text{A}$ ) to vary the effective mechanical pre-strain of the actuator film, allowing a 7 $\times$  to 10 $\times$  change in stiffness [22] (fig. 2.11).

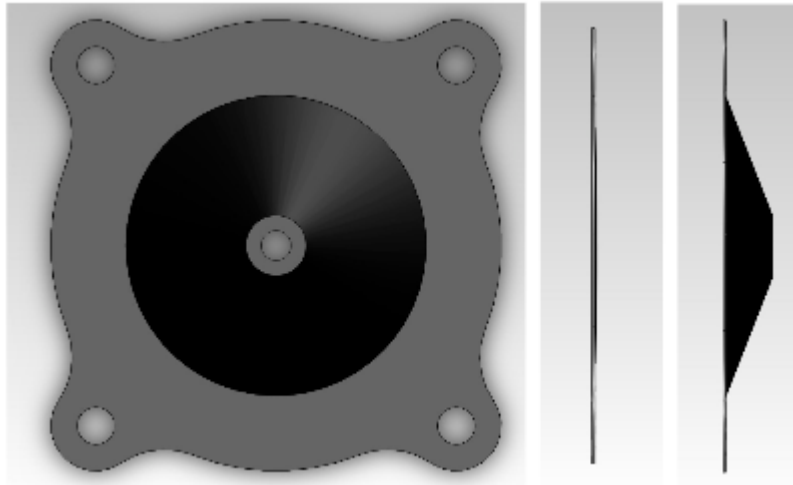


Figure 2.11: EAP actuator design: view from above, rest state, activated state, from [22]

### Rheological fluids

Magnetorheological (MR) and Electrorheological (ER) fluids change their viscosity when subjected to, respectively, a magnetic and an electrical field. Their resistance to strain increases with this external field. These fluids are composed of micrometric scale particles, and to obtain better effects with low fields values one can split the MR fluid into microchannels. They only stiffen in the shear direction, so any tensile force is not handled.

For instance, a mechanism based on bellows filled with rheological fluid can change the stiffness of the device presented in [23] (fig. 2.12).

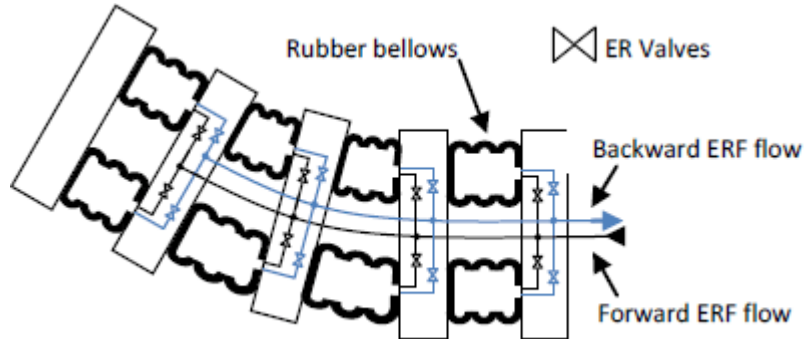


Figure 2.12: Soft fluidic continuum arm: flexibility control through ER fluid flow, from [23]

### Magnetostrictive materials

Some ferromagnetic materials change their shape or dimensions during the process of magnetization. There is a bi-directional coupling between their magnetic and mechanical states, providing both actuation and sensing effects. These materials also exhibit a reduction in their effective elastic moduli during magnetic domain rotation, due to the superposition of purely elastic strain and magnetoelastic strain. This effect enables the development of tunable stiffness components, which can be applied to a variety of vibration control problems. The key advantages of magnetostrictive materials are non-contact operation, very high reliability, high bandwidth, and inherent active behaviour.

Like in piezoelectric materials, a change in the magnetic boundary condition from constant magnetic field (magnetically free condition) to constant magnetic flux density (magnetically blocked condition) causes an increase in Young's modulus of magnetostrictive materials. This effect is used, for instance, to tune the resonant frequency of vibration absorbers.

In [24] J. Scheidler et al. proposed a tunable stiffness spring relying on magnetostriction: the device enables in situ stiffness tuning for vibration control applications (fig. 2.13).

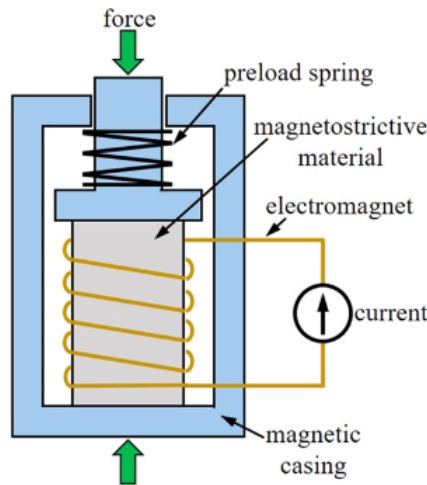


Figure 2.13: Variable stiffness spring using magnetostrictive material, from [24]

### Electrostrictive materials

Electrostriction is a property of dielectric materials, causing them to change shape, to deform under the action of an external electric field. The resulting strain is proportional to the square of polarization. Reversal of electric field does not reverse the direction of deformation. An example of electrostrictive material can be lead magnesium niobate (PMN), which is often used for actuators that need a larger displacement than piezoelectric materials can achieve.

### Biomaterials

Some biomaterials can show effective change in stiffness. The echinoderms (for instance, the sea cucumbers or the starfish) can modify the stiffness of their skin through quick and reversible collagen fiber linking. The interactions of the collagen fibrils can be regulated by their nervous system such that the stress transfer is modified and therefore the stiffness.

A nanocomposite polymer reinforced with cellulose fibers inspired by the ability of the skin of sea cucumber to change its stiffness is presented in [25]. In natural state, the result is rigid due to the interactions of nanofibers through hydroxyl groups. Lowering down these interactions by a chemical regulator leads to a decrease in stiffness.

## 2.2.2 Structural interactions

In this case the material is composed by several elements, which interactions determine the overall behaviour of the structure. Generally, an equivalent homogeneous material is considered. There are three main types of mechanisms that show the mentioned working principle: bulk locking (granular jamming, turgor pressure), longitudinal locking (layer jamming, wire jamming), segments locking (through wires, bellows, or soft layers).

- Bulk locking: these mechanisms are made by a solid solution composed of several elements in its volume (in both the longitudinal and lateral directions). Stiffness change is obtained by modifying the interactions of all these elements. The size of elements compared to characteristic dimensions of the structure can range from relatively large (discrete deformation and shape-locking) to very small (almost continuous deformation and shape-locking). With this solution, it is possible to deform the structure in the flexible state and to lock it in a given configuration when switching to the rigid state. The change of interactions can be obtained by electro-magnetic field, pressure difference, force application or chemical reaction [3].
- Longitudinal locking: In this configuration the solution is divided into several elements over its section. Like in the previous solutions, change of stiffness is obtained by modifying the elements interactions. These interactions are longitudinal with respect to the structure, and the activating stimulus can be a pressure difference or a force application. With this solution, it is also possible to deform the structure in the flexible state and to lock it in a given configuration when switching to the rigid state.
- Segments locking: in this case the structure is divided into several elements only over its length, such that only one element lies in the cross section. Bending behaviour is changeable by modifying the interactions of these segments, which are usually locked by the tension of longitudinal cables. Other locking mechanisms can be magnetic field or pressure difference.

## Granular jamming

The most known application of bulk locking mechanisms is granular jamming: basically the structural stiffness of a granular material embedded in a membrane can be modified via pressure difference across the membrane. At ambient pressure relative motion between the particles is allowed, resulting in a compliant structure. By increasing the pressure the grains start to lock with each other, leading to a more rigid system.

One advantage is the very small volume variation between the soft and stiff states, but one disadvantage is the total volume which, spread in all three dimensions, make this solution less suitable for thin mechanisms.

Granular jamming finds application for instance in soft robotic grippers, and the most common pressure source comes from pneumatic systems (fig. 2.14).

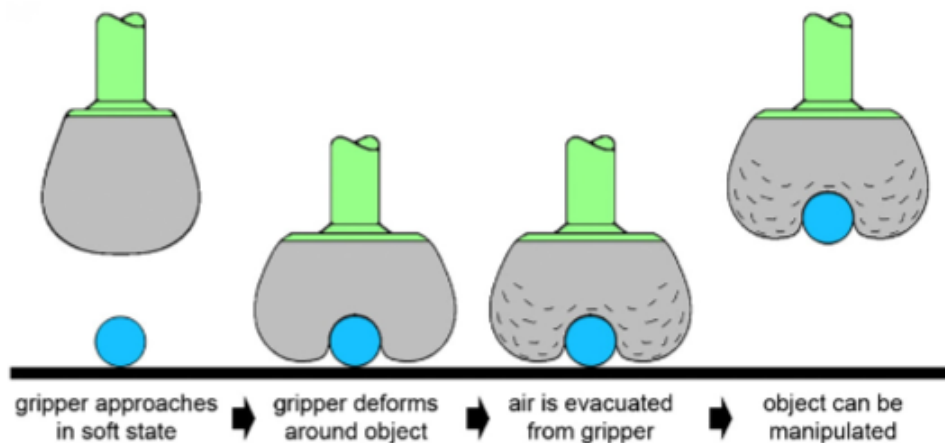


Figure 2.14: Granular jamming robotic gripper, working principle, from [26]

## Turgor pressure

Another solution based on bulk locking is similar to the turgor pressure in plants: they can increase the elastic modulus thanks to a pressure exerted by the incompressible fluid filling the cells. Basically it is sort of granular jamming where the locking mechanism come from fluid pressure inside grains. There exist models in which cells are considered as elastic membranes filled with water, or models based on foam with closed cells filled with fluid. These

models can estimate the elastic modulus as a function of the turgor pressure. This is still a research field, and no working mechanisms exist yet basing on this solution. Anyway, to give an example, in [27] they presented a variable stiffness solution using dielectric elastomers and fluid which is inspired by something really similar to turgor pressure.

### Layer jamming

Longitudinal locking solution where the longitudinal elements are thin plates: they can slide over each other in the flexible state, while in the rigid state they are locked by frictional force or shape conformity (with texturized surfaces or specific geometries that lock with each other when the elements are mechanically coupled). The main difference between a single material multi-layer beam and a layer jamming beam is that in the latter a single segment does not spread along the whole beam length: there are many elements overlapped. Layer jamming mechanisms are lightweight and characterized by small space occupation and high design flexibility. These mechanisms can be activated through pressure difference, pneumatically [28], or electrostatically. T. Wang et al. proposed a layer jamming technique for soft robotics called Electrostatic Layer Jamming (ELJ) (fig. 2.15) [29]. The locking mechanism is caused by friction between layers, due to an external electrostatic force. The high voltage required is not a huge problem thanks to the small lightweighted high voltage commercial modules in the market, and electric control is easy to integrate. Unlike the pneumatic case (PLJ), the pressure on each contact surface may be different depending on the design. Friction coefficient, and then stiffness, are function of the external voltage.

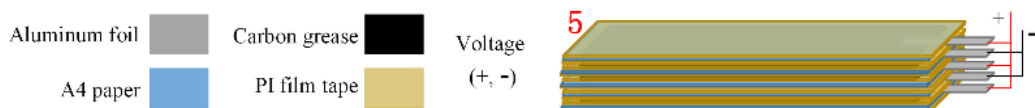


Figure 2.15: ELJ beam composition, from [29]

## Wire jamming

Longitudinal elements are wires: they can be free to move, giving a flexible structure, but once they are locked by an external force, as their lengths are fixed, the shape is locked and the stiffness is increased. It is a less common solution than layer jamming (fig. 2.16).

Example of a medical device relying on this concept can be found in [30].

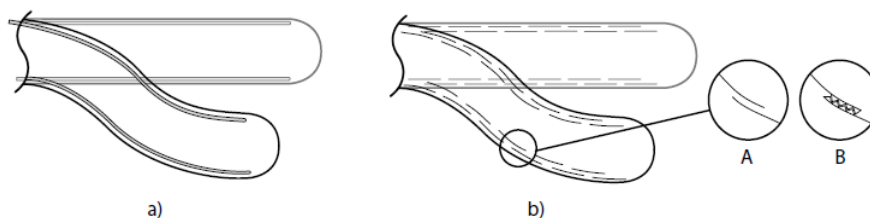


Figure 2.16: Wire jamming (a) vs layer jamming (b), from [3]

## Segments locking

Elements occupy the whole structure cross section. They can be locked through 3 main methods: wires, bellows, soft layers (fig. 2.17).

- **Wires:** tension of several wires or a single central wire allows the segments locking and induces the required stiffening. Segments can be beads, cylindrical elements connected by spherical joints or rigid cylindrical elements. Stiffness variation comes from friction between elements, due to the tension in the cables. Tensioning of multiple wires is already used for tip control of medical devices or snake-like robots. J. Kim et al. proposed a snake-like manipulator basing on this concept, for minimally invasive surgery applications (fig. 2.18) [31]. Y. Jiang et al. presented a “chain-like granular jamming” solution which can be actually classified in this section. They optimized segments shape and showed a bigger relative stiffness increment of the wire-actuated solution with respect to a vacuum-actuated one, respectively 50x vs 2x [32].

- Bellows: elements composing the structure are bonded with bellows-like connectors: in this way segments can be locked with a defined angle, by actuating the bellows differently [3]. Hybrid example in [23].
- Soft layers: in this case the inter-segment is made of soft material, capable of a full section locking. The global structure is similar to a multi-layer beam, but layers lay in the transversal direction. Stiffness of the multi-layer structure (a rubber layer between two rigid plates) can be modified by its compression, usually given through tensioned cable, like in [33]. The overall deformation could be discrete or almost continuous, depending on the size of segments. With this solution it is even possible to deform the structure in the flexible state, and to lock it in a given configuration when switching to the rigid state.

An alternative activation method to obtain segments locking is by sliding a element with respect to a fixed one. M. Jiang presented a type of laminates which can show variable stiffness thanks to a concept called “sliding layer” [34]. Laminate structure is composed by three layers. Every layer is made alternatively by rigid and soft segments. When layers are aligned a soft structure is obtained, which stiffens as the central layer is shifted such that there are no more section made only by compliant material (fig. 2.19). From a different point of view this solution could be also seen as a multi-layer beam or a layer jamming mechanism. This concept has been tested in various scenarios, including variable stiffness flapping fins. A similar concept is also studied in [35].

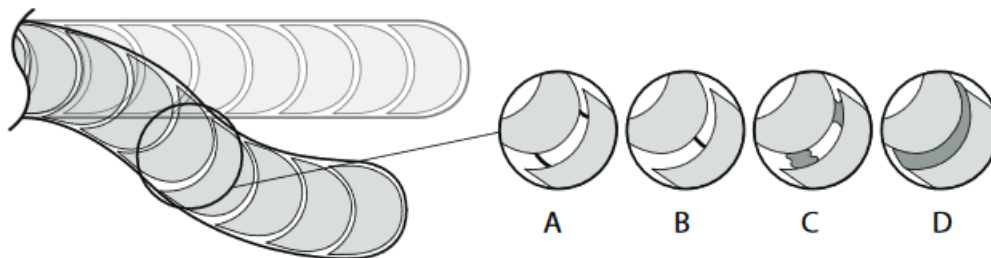


Figure 2.17: Segments locking concept using wires, bellows, soft layers, from [3]

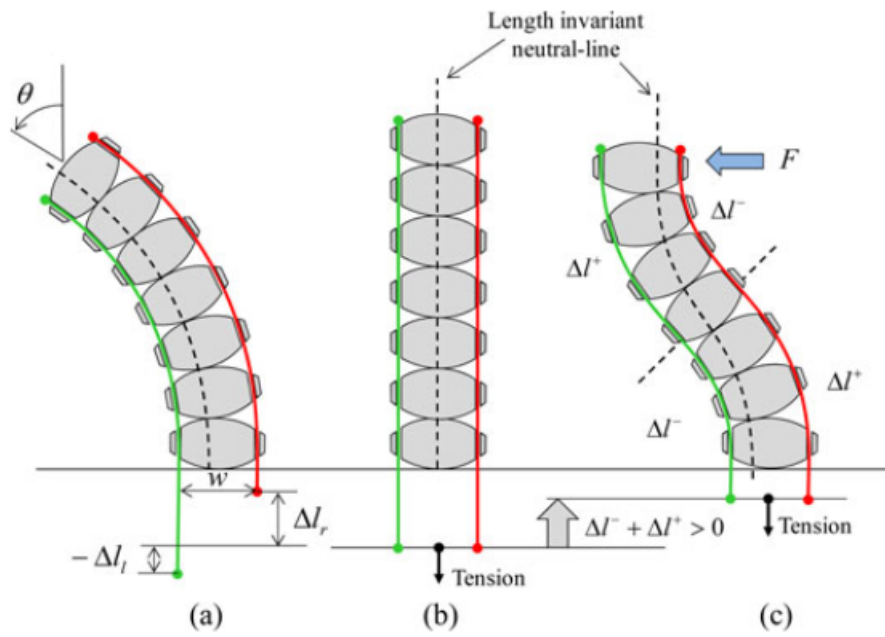


Figure 2.18: Snake-like robot concept by using wires segments locking, from [31]

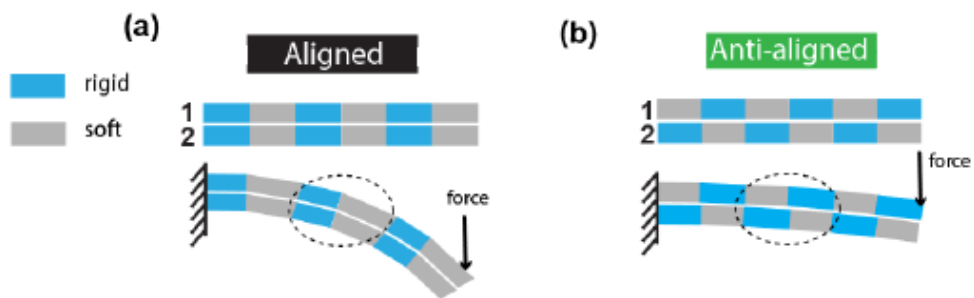


Figure 2.19: Sliding layer concept, from [34]

## 2.3 Actuator-like solutions

These methods rely on movement, of a component or a fluid, to achieve variable stiffness characteristics.

### 2.3.1 Fluid-based solutions

#### Pneumatic

This controllable stiffness solution can be based on silicone air-pressurized chambers, with a braided reinforcement to avoid volume expansion due to pressurization. In pneumatic expansion the working principle is a cross section change, while here volume should be kept almost constant in time.

A. Stilli et al. presented a stiffness-controllable robot link concept that implements this solution (fig. 2.20) [36].

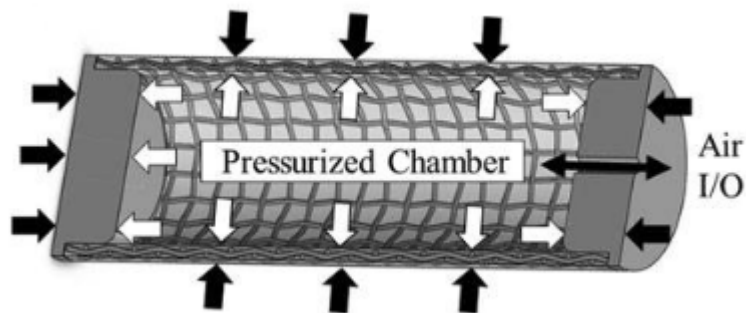


Figure 2.20: Pneumatic robot link with plastic and silicone chamber, from [36]

#### Hydraulic

Stiffer and more robust solution with respect to pneumatic actuations, which are in general more compliant and have potential for safer physical human-robot interactions.

In [37] a review of hydraulic muscles as an alternative of pneumatic actuations is presented.

## Fluidic flexible matrix composites

FFMCs are composite materials where fluidic channels are embedded in a matrix. When the fluid (water, oil) is free to flow through the channels then a soft state is obtained. Stiff state is achieved by closing the entry valve, increasing the fluid pressure and the global rigidity [38]. Such blocked state can resist large forces with low pressure in the fluidic network.

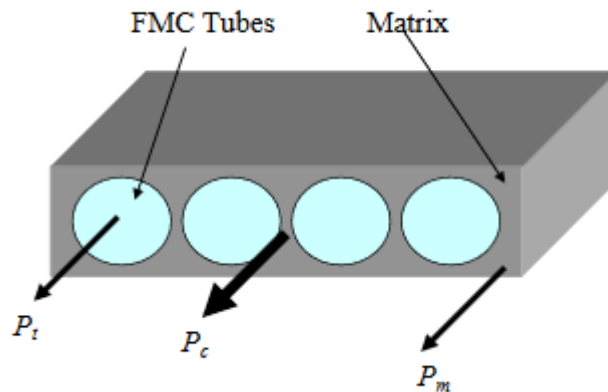


Figure 2.21: FFMC: pressure is shared between tubes and matrix, from [38]

## 2.3.2 Mechanical solutions

### Component translation/rotation

These solutions allow to achieve stiffness variation of a system by the movement of certain components. For instance, the variation in length of a lever arm with a spring can lead to the modification of the effective stiffness observed at the end of the arm. This solution is used in revolute joints for robotic applications. Furthermore, a structure which stiffness relies on some rigid components sees its flexural/torsional behaviour varied when such components translate or rotate within the structure.

An example of a variable stiffness actuator working thanks to lever arm length variation is the “vsaUT-II”, presented in [39]. It is system with a single degree of freedom, where the hollow lever arm can only rotate, but the pivot point is able to translate via a gear mechanism (fig. 2.22).

M. Amprikidis and J.E. Cooper proposed “smart spars” to control the torsion

of an aircraft wing [40]. The aeroelastic behaviour of aerospace structures, in particular static deflections, can be controlled as desired through changes in position, orientation and stiffness of the spars. Translational and rotational movements can lead to variations in the torsional and bending stiffness as well as shear centre position. Smart materials suffer from limits in the amount of force required to twist a full scale wing. The idea is that of making use of aerodynamic forces acting upon the wing to provide the moment to twist the wing. Two approaches have been tried: two fixed spars with one moveable spar in between, and two rotating spars (fig. 2.23). It has been proved that one can easily vary the wings twist through these spar movements, but the results are not general, they highly depend on the type of structure used.

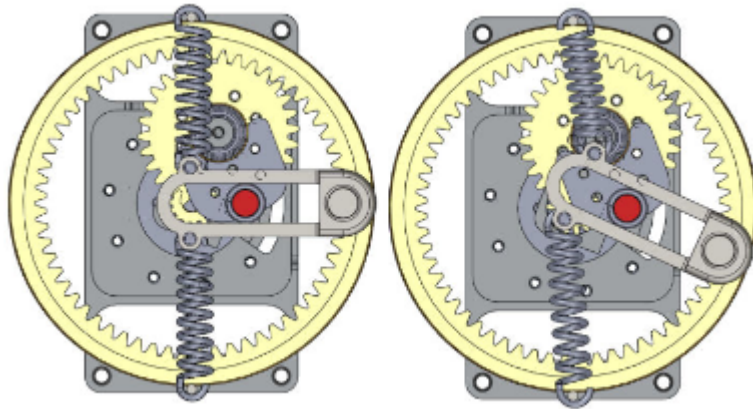


Figure 2.22: vsaUT-II: variable lever arm length concept, from [39]

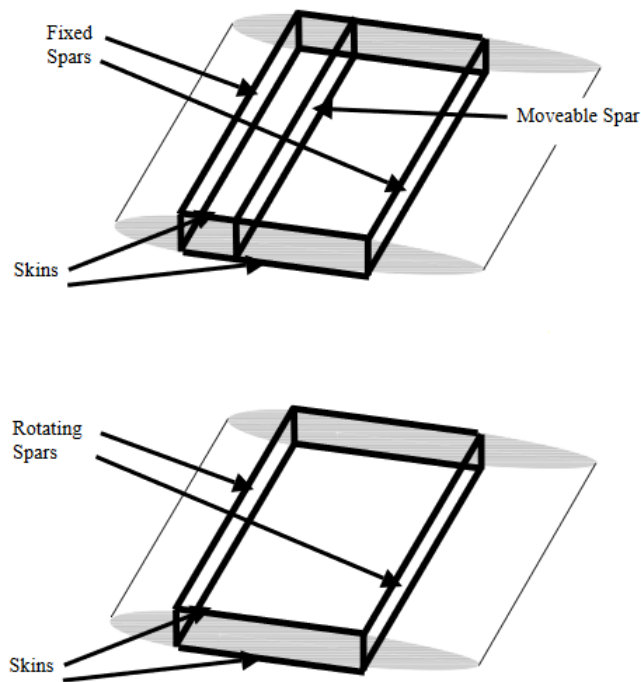


Figure 2.23: Moving wing spars to obtain an adaptive airfoil, from [40]

### Antagonistic approach

A mechanical approach to obtain tunable stiffness joints is an antagonistic arrangement, similar to human muscle actuation. This systems show a single degree of freedom. Two actuators are mounted in an opposed manner at the joint, each able to pull and thereby exert torques in one direction. Motors are connected using non-linear springs. A link motion is induced if only one motor pulls. If both motors pull (co-contraction) the joint, stiffness increases due to the increasing actuator stiffness. It is also possible to use not only rotational motors.

In [41] a review of possible configurations to obtain variable stiffness by using motors and springs is showed. Motors can be antagonistic (fig. 2.24) or independent from each other (fig. 2.25).

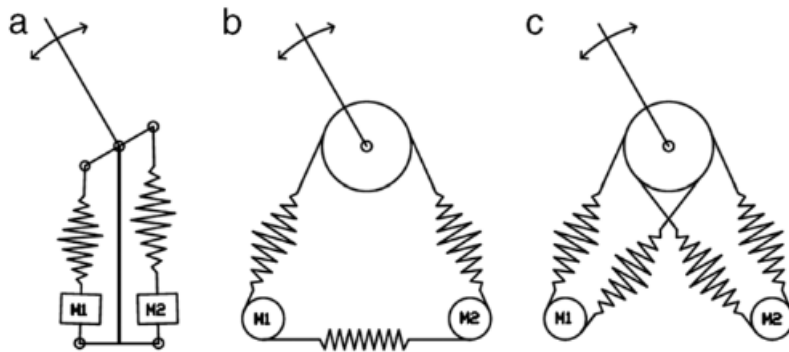


Figure 2.24: Antagonistic approach: antagonistic motors, from [41]

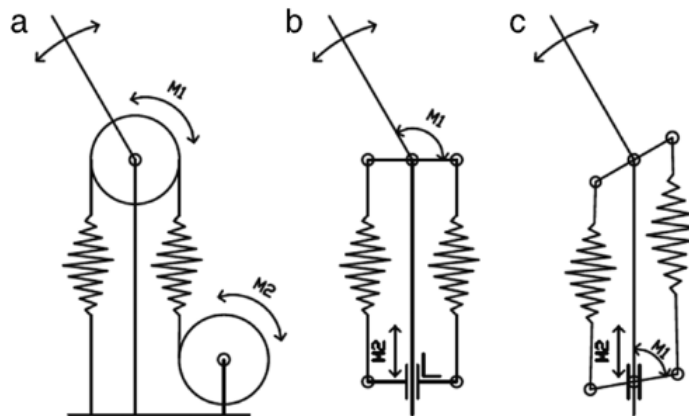


Figure 2.25: Antagonistic approach: independent motors, from [41]

## Muscles

Some of the solutions previously described (e.g. pneumatic) can be classified as artificial muscles, namely components capable of contractive movements. This paragraph wants to make the reader aware that muscles relying on different principles, such as chemical reactions or nanotechnology, do exist. The change of stiffness during the contraction phase is one of the most important characteristics of muscles. This is an active research field, and polymer

artificial muscle technologies are being developed that produce strains and stresses using electrostatic forces, electrostriction, ion insertion, and molecular conformational changes. Materials used include elastomers, conducting polymers, ionically conducting polymers, and carbon nanotubes (example in [42], fig. 2.26).

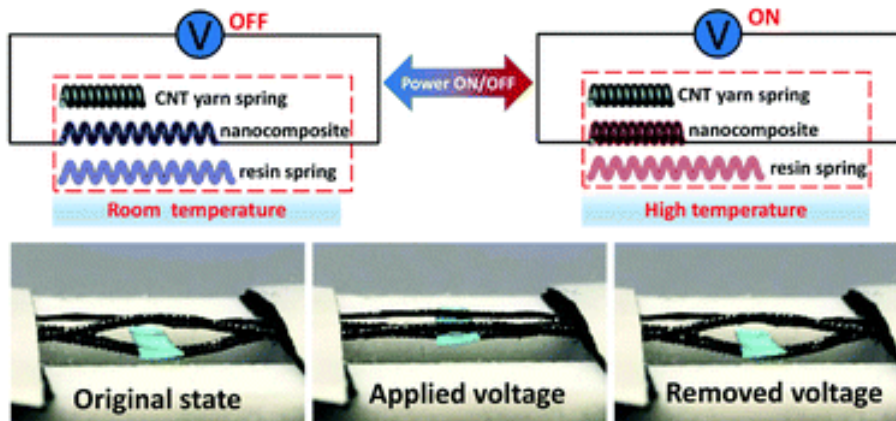


Figure 2.26: Variable stiffness carbon nanotube spring-like nanocomposite yarn for artificial muscles, from [42]

## 2.4 Hybrid

A combination of the previous solutions leads to hybrid solutions. For example, it is possible to change material properties between some rigid links to ensure a controllable stiffness device. The locking of structural elements can be obtained with rheological fluids or phase transition materials.

The method presented in [23] and shown in fig. 2.12 is actually hybrid: electrorheological fluid and bellows segments locking solutions are mixed to achieve the result.

An interesting device combining vacuum activated layer jamming and component translation is showed in [43]. The tendon driven manipulator is basically composed by a compliant external layer with circular section and a

honeycomb core with jamming layers. When vacuum is applied stiffening occurs where jamming layers are positioned, but thanks to a sliding mechanism these positions can be controlled by the user, allowing for various stiff configurations (fig. 2.27).

The author wants to highlight that some of the described concepts could be inserted in multiple sections of this chapter, due to their hybrid characteristics. In such cases, the main working principle is used as discriminant. For example, the mechanism presented in [33] works thanks to a tendon driven actuator. For this reason it could be inserted in section 2.3, but stiffening actually occurs due to locking of segments connected in series. That's why the correspondent paragraph is 2.2.2. The same happens for sliding layer laminate structure [34], where segments are locked via mechanical translation.

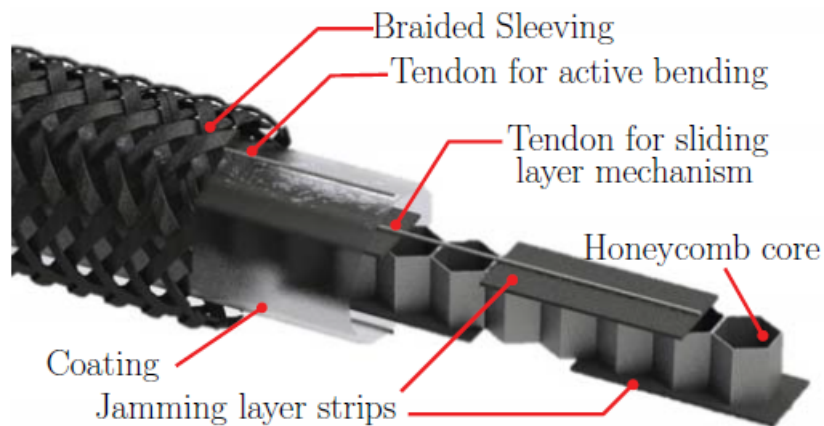


Figure 2.27: Hybrid solution: mechanical translation and layer jamming, from [43]

# Chapter 3

## Solutions comparison

The following step, after reviewing the existing solutions, is their comparison.

In this chapter project requirements are defined and used for a first classification. Then follows the definition of project objectives and objectives-based comparison of remaining solutions.

Since the final goal is related to the study of concepts for research purposes, like mentioned in chapter 1, the following comparison is based on possible suitable flapping wing implementations of listed technologies. Moreover, next to project requirements and objectives, other design constraints are represented by availability of materials or possible dangerous procedures.

### 3.1 Requirements-based comparison

A project requirement is a fundamental design constraint, usually a quantitative value, as precise as possible. The only options about a requirement are “satisfied” or “unsatisfied”, and the chosen solution must satisfy each set requirement.

In this project numerical requirements are set, but sometimes it is difficult to say if they are satisfied by a certain technology, because of the many possible ways and methods in which a solution can be implemented.

Here follows the list of project requirements about the design of a mechanism

to achieve variable stiffness in a flapping wing.

- Mass: total mass of Robird is  $\sim 730$  g. Most of it is concentrated in the bird body. Therefore the wing, now composed by a stiff structure inserted in an expanded polystyrene matrix, should keep a weight of  $10^1$  g of order of magnitude. Each Robird wing flaps thanks to a pair of spars of different length, connected to the motor group. These elements are made of titanium and carbon, and are inserted in plastic tubes. Masses of the two spars, excluding the parts constrained in bird's body, are 13.1 g and 11.5 g.
- Speed: stiffness change should be quick, both for testing purposes and for an effective implementation in Robird's wings. Considering a wing beat frequency of about 5 Hz, stiffness variation should take from one to few (ca. 3) wing beats, then activation time range should be  $0.1 \div 0.7$ s.
- Size: the actual wing is considered as "boundary condition" for the new component. Its area is  $\sim 650$  cm<sup>2</sup>. It is approximately composed by a  $20 \times 15$  cm rectangle and a  $20 \times 35$  cm right triangle. Thickness at wing root goes from 1.4 cm near the leading edge to 0.2 cm at the trailing edge. Leading edge thickness decreases up to 0.5 cm at wingtip, while trailing edge thickness stays constant in the spanwise direction. The solution must fit in this volume. Furthermore, cantilever wing spars length are of 250 mm and 325 mm, with maximum diameters of  $\sim 4$  mm, excluding the plastic tube in which they are inserted.
- Reversibility: the stiffness variation should be bidirectional. Chosen solution must be able to switch between rigid and soft state and viceversa.
- Repeatability: the designed component must be able to perform stiffness changes in the same way throughout its life cycle, which must comprise several flights.

Requirements-based comparison of the existing solutions is described in table 3.1. Where possible, it is based on numerical data found in literature.

Solution	Requirements				
	Mass	Speed	Size	Reversible	Repeatable
Origami structures	Y	/	N	Y	Y
Pneumatic expansion	N	Y	N	Y	Y
Multi-stable structures	/	Y	Y	Y	Y
<u>Multi-layer beams</u>	Y	Y	Y	Y	Y
<u>Piezoelectric materials</u>	Y	Y	Y	Y	Y
Low melting point materials	Y	N	Y	N	Y
Wax	Y	N	Y	N	Y
Solder	Y	N	Y	N	Y
Shape memory materials	Y	N	Y	N	Y
Electroactive polymers	Y	Y	Y	Y	Y
<u>Rheological fluids</u>	Y	Y	Y	Y	Y
Magnetostrictive materials	/	/	/	/	/
Electrostrictive materials	/	/	/	/	/
Biomaterials	/	/	/	/	/
Granular jamming	/	Y	N	Y	Y
Turgor pressure	/	/	/	/	/
<u>Layer jamming</u>	Y	Y	Y	Y	Y
Wire jamming	Y	/	/	Y	Y
<u>Segments locking</u>	Y	Y	Y	Y	Y
Pneumatic	N	Y	Y	Y	Y
Hydraulic	N	Y	Y	Y	Y
Fluidic flexible matrix composites	N	Y	Y	Y	Y
<u>Component translation/rotation</u>	Y	Y	Y	Y	Y
Antagonistic approach	/	Y	/	Y	Y
Muscles	/	Y	/	Y	Y

Table 3.1: Requirements-based comparison. “Y” and “N” represent “satisfied” and “not satisfied”, respectively.

Considering global feasibility and possible implementations, from the requirements-based comparison 4 solutions are chosen for next classification:

- Multi-layer beams with electrostatic activation (EBL)
- Electrostatic layer jamming (ELJ)
- Segments locking
- Component translation/rotation

Considerations about other technologies: mechanisms relying on piezoelectric effect are usually utilized in actuators where very small strokes are needed, lack of possible implementations indeed occurs. About rheological fluids: these materials are in general still too compliant for this application, even in their stiffer state.

## 3.2 Objectives-based comparison

A project objective is a more qualitative design constraint. More than two options are allowed for each objective.

Objectives are ranked and weighted, in order to assign a score to solutions, a numerical value which allows a better comparison.

Here follows the list of project objectives about the design of a mechanism to achieve variable stiffness in a flapping wing.

- Easy to do: quite important constraint, in terms of time, materials and experience needed to build specimens or prototypes.
- Low power consumption: for instance, power directly determines size and weight of batteries given a certain flight time. Viceversa, a high power consumption reduces the flight time given a certain type of battery.
- Low number of additional components: it has to stay low not to increase mass and volume encumbrance.
- Smooth stiffness variation: a smooth stiffness change is preferred with respect to a dual stiffness solution, allowing for in-between values.

- High strength-weight ratio: the mechanism should be durable and able to bear loads while keeping a low mass, obvious objective for a flying robot.
- High strength-volume ratio: the mechanism should be resistant while fitting in the given volume.
- Low cost: it has to be considered that Robirds are on the market, and the cost of this solution should be reasonable and related to the obtained results. Cost sets a limit in terms of feasibility and testing, too.
- Wide stiffness range: generally large stiffness variation are a better result. This parameters depends on the type of implementation: e.g., if one thinks of a variable stiffness wing spar, then a good result can be a stiffness range that reaches values below and above the current spars stiffness. Shorter spar, which is the most rigid one due to the smaller length, shows an approximated bending stiffness of 913 N/m related to a concentrated tip force, and 2434 N/m related to an evenly distributed load, considering cantilever configuration for both cases. Certainly a lower limit does exist for stiffness, due to a certain load bearing capability the structure should maintain in every configuration.

Once objectives are listed a ranking by importance is made. Table 3.2 has to be read by column: “1” means that column solution is more important than row solution, “0” means that it is less important. Then column values are summed up and a ranking from 1 to 8 is made. Finally weights are set by shifting the ranking to a 1-20 scale to emphasize gaps between different project objectives.

Comparison is structured in this way: every solution cast a grade from 1 to 4 for each project objective, which signifies, respectively, “weak”, “satisfactory”, “good”, “excellent”.

Objective-based comparison can be seen in table 3.3. Votes are weighted and summed up to obtain the final scores.

	Easy	Power	Comp	Smooth	S/W	S/V	Cost	St range
Easy	/	1	0	0	0	0	0	1
Power	0	/	0	0	0	0	1	0
Comp	1	1	/	0	0	0	1	1
Smooth	1	1	1	/	1	1	1	1
S/W	1	1	1	0	/	1	1	1
S/V	1	1	1	0	0	/	1	1
Cost	0	0	0	0	0	0	/	1
St range	1	1	0	0	0	0	0	/
<b>Sum</b>	5	6	3	0	1	2	6	5
<b>Ranking</b>	6	8	4	1	2	3	7	5
<b>Weight</b>	17	20	10	1	4	5	18	14

Table 3.2: Objectives ranking

<b>Objectives</b>	<b>Solutions</b>				<b>Weight</b>
	EBL	ELJ	Segments	Transl/rot	
Easy	1	1	3	4	17
Power	1	1	3	4	20
Comp	2	2	2	2	10
Smooth	4	4	1	3	1
S/W	3	4	4	2	4
S/V	2	3	2	3	5
Cost	3	3	4	4	18
St range	3	3	4	3	14
<b>Score</b>	179	188	286	308	

Table 3.3: Objective-based comparison

By comparing the scores it can be noted that electrostatics-based solutions are less interesting especially because of the first two objectives. First of all, the main obstacle is represented by high voltage: even a simple static test would involve lots of people, responsibilities, safety measures and at least some experience in this field would be needed for it to become feasible. Secondly, both electrostatic mechanisms are inherently very soft: it is expected that a certain voltage would be applied for most of the flight time, utilizing a lot of power, in contrast with Portwings project objectives.

In the following sections the remaining concepts, i.e. segments locking and component translation/rotation, are further investigated and tested. Speaking about implementation, these solutions suit well as “smart spar”, since they are usually implemented as beam-like structures.

The idea of a smart spar is a good option to vary Robird wing stiffness:

- Smart spar is an existent concept in literature ( [12], [11], [40] ) and offers the possibility to be implemented in terms of both flexural and torsional stiffness.
- In current Robird design wings are prevalently constructed by using expanded polystyrene, i.e. a light and compliant foam. External surfaces are covered by a polymeric resin layer. In each wing two rigid round section spars, made using titanium alloy, carbon and an internal steel spring are inserted in the foam matrix. These components are connected to the motor group and allow wings to flap. Spars are the stiffest wing components: global wing stiffness is highly influenced by the one of longitudinal spars.

In the next chapters two solutions to obtain a beam characterized by variable bending stiffness are analysed, based on linear translation and rotary motion. Methods include experimental tests for both analysed concepts.

# Chapter 4

## Modelling and Design

In this chapter the two chosen solutions are described.

In particular, the first concept to be introduced is a novel solution based on the pure translation of an inner rod inside an outer tube, both showing multiple cross section properties or material properties, that can lead to a beam with tunable stiffness. About this concept, a simplified mathematical model is defined, too. The second studied solution is based on the pure rotation of a non-axial symmetric beam.

### 4.1 Sliding segments

The first investigated concept is a novel hybrid solution based on segments locking and component translation. It merges the two solutions with highest scores in the objectives-based comparison.

In this section the design process is illustrated, and a simplified analytical model is introduced.

#### 4.1.1 Segments locking device

A consolidated segments locking variable stiffness medical device is shown in fig. 4.1. The segments locking concept is shown in section 2.2.2. Here segments consist of spheres alternated with cylinder-like shapes. Tension of an internal wire activates frictional locking in whatever spatial configuration,

achieving remarkable rigidity. The mechanism includes several internal components, including springs and screws, to adjust wire tension. Similar concepts also find application in the fields of manufacturing, e.g. as manipulators for cooler nozzle position control in CNC machining. Its stiffening performance is impressive, but it presents some disadvantages related to a flapping wing application: in stiffer states it is substantially a single rigid body with variable force threshold to become a set of spherically connected smaller segments. For this reason this specific segments locking approach for a smart flapping spar loses one of its major advantages: it cannot exploit its whole stiffness range, because when the internal cable is not tensioned, the presence of a set of disconnected bodies in an ambient with such high dynamics is not recommended (because of impacts between the uncoupled segments and issues due to vibrations), and probably too compliant for the application. Moreover, this kind of device cannot restore a straight configuration after deformation by only using one degree of freedom (cable tension). Solutions based on this concept are still suitable, but, for these reasons, segments should be designed such that they remain more connected to each other even in the most compliant configurations, e.g. by placing elastic inter-segment layers (see 2.2.2).



Figure 4.1: Acrobat SUV Vacuum Stabilizer: provides local stabilization of a target vessel during off-pump coronary artery bypass, from [www.getinge.com](http://www.getinge.com)

### 4.1.2 Novel solution

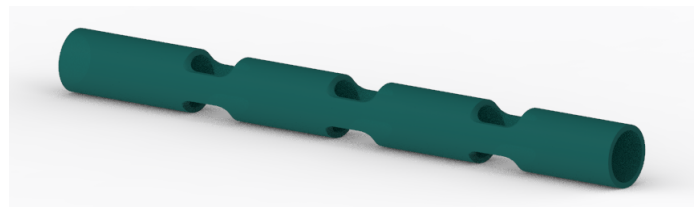
The previous medical device can give interesting insights. By connecting the outer cylinders to each other, as well as the inner spheres, and by eliminating the cable one can obtain two beam-like elastic bodies, in particular a rod and a tube, which can translate with respect to each other to achieve stiffness changes. The concept is shown in figures 4.2 and 4.3, which show a rendering of a first sample and side views focusing to the sliding segments mechanism. Basically this concept is based on flexure shifting, with beam-like elements. Flexures are in general compliant links, relying only on elastic deformation to allow motion in some directions, while providing load-carrying support in others [44]. Studies about a really similar concept can be found in [34] and [35]. The main difference with [34] is that in this case the structure is not a laminate: it is a tubular component, globally stiffer (stronger cross sections) and suitable for the application, and allowing possible additional rotary movements (showed in the next chapter).

In constant sectioned beam-like elements, flexural stiffness is usually represented by the  $EI$  product, where  $E$  (MPa) is the material Young's modulus and  $I$  ( $\text{mm}^4$ ) is the cross section second moment of area.

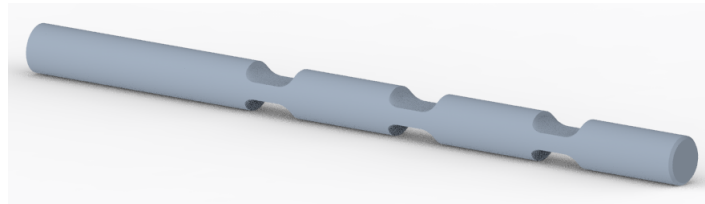
Therefore, for these kind of elements, one can generate flexures both by changing the material properties and by modifying the cross section.

In first built samples flexures are represented by those beam segments which exhibit more compliant cross sections regarding bending in a certain direction, while in another specimen smaller flexural rigidity is given by different material properties. Connections between tube segments and between internal rod segments are considered in this way. When rod and tube flexures are aligned a compliant elastic structure is obtained, but when internal rigid segments are shifted in correspondence of external flexures the beam should reach a bigger bending stiffness. By shifting the inner rod, flexures are replaced by stronger sections. Moreover, rod rigid segments should also constraint tube flexible segments from deforming, and that is why this is a kind of segment locking (see fig. 4.3).

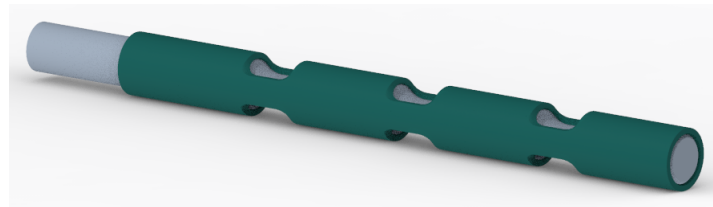
It has to be noted that these samples aim is to test the concept of sliding segments, they do not have to satisfy all project requirements yet.



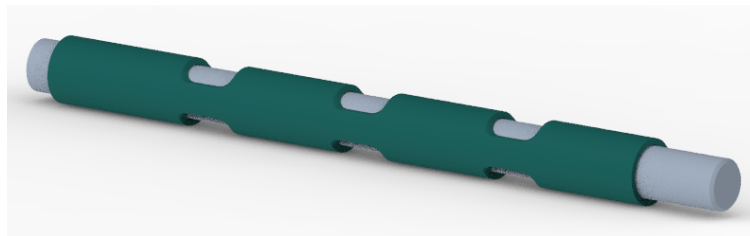
(a)



(b)

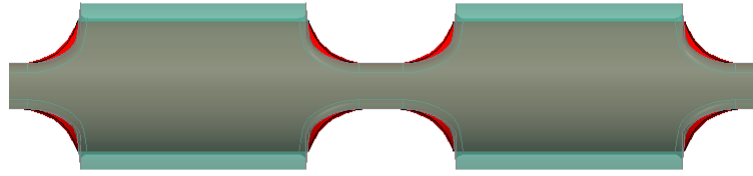


(c)

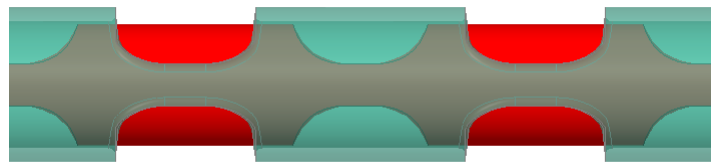


(d)

Figure 4.2: Images of sliding segments sample: (a) outer tube, (b) inner rod, (c) compliant unshifted configuration and (d) rigid fully shifted configuration



(a) unshifted



(b) shifted

Figure 4.3: Sliding segments concept

### 4.1.3 Simplified analytic model

Euler-Bernoulli beam theory is used to analytically describe structure behaviour under static bending loads.

Single elastic body assumption is taken as hypothesis: this means that in this first model every predicted behaviour is due to pure cross section and material properties, neglecting interactions between different bodies.

Thus, it is to be highlighted that this model does not claim to precisely describe bending behaviour of multi-components beam structures: since sliding segments is a novel concept, a first try simplified linear model is a good way to start. It might also be able to show trends and practical limitations. Its comparison with experimental results can give insights on how the model can be improved in future works.

In this case transversal dimensions can be set way smaller than longitudinal one: this satisfies the thin beam requirement (length to thickness ratio  $> 10$ ), and makes this theory applicable almost without loss of accuracy due to negligibility of shear effects.

Euler-Bernoulli beam theory is based on two principal assumptions:

- Plane sections remain plane: any beam section that is a flat plane before deformation is assumed to keep a plane geometry after beam deforms. This is in general relatively valid for bending beams, unless the beam experiences significant shear or torsional stresses relative to bending ones. Shear stresses may become large relative to bending stresses in cases where section dimensions are not negligible with respect to beam length.

This hypothesis also assumes that any cross sections perpendicular to the neutral axis before the beam deforms remain perpendicular to the neutral axis after deformation.

- Deformed beam angles are small: this assumption leads to a few benefits from a calculation standpoint. As one can see in fig. 4.4, if  $x$  represents the location along beam axis and  $v(x)$  is the displacement due to bending at location  $x$ , then slope of the beam, thanks to this assumption, can be given by

$$\theta \sim \tan \theta = \frac{dv}{dx} = v' \quad (4.1)$$

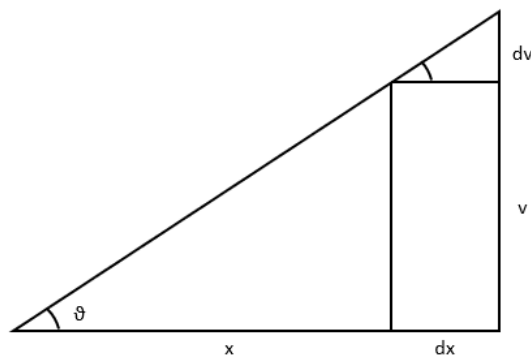


Figure 4.4: Small deformed beam angles hypothesis

Based on the assumptions discussed above, Euler-Bernoulli beam theory leads to differential equation 4.2, which can be integrated to obtain the elastic line of a beam subjected to bending loads. Boundary conditions to perform the integration are derived from how the beam is constrained at its ends. In this case beam is bounded in cantilever configuration, with fixed-free ends. This constraint is suitable for a possible application within a flapping wing, where the fixed end would be attached to bird body, or flapping set-up to perform aeroelasticity wind tunnel tests.

Here  $M(x)$  (Nm) is the function representing bending torque along beam length  $x$  (mm), generated by external loads, and  $v$  (mm) indicates vertical beam displacement. It is important to highlight that this equation can be used to solve homogenous beams with constant cross section and linear elastic materials. It can't be used when large deflections occur and the problem becomes non-linear.

Furthermore, clearance and other multi-body effects are not included in this model, due to single elastic body assumption.

$$v'' = \frac{d^2v}{dx^2} = \frac{M(x)}{EI} \quad (4.2)$$

## Implementation

Solution presented in section 4.1.2 could be seen as a beam with variable cross section, therefore the structure is modelled as several beam segments connected in series. One segment with constant cross section corresponds to one static beam equation in the form 4.2. This leads to a second order system of ordinary differential equations, solvable in closed form.

Every second order equation needs two boundary conditions to be integrated. To represent cantilever configuration, rotation angle and displacement are imposed to be zero at  $x = 0$ . These are the two boundary conditions for the first segment.

Then, for a generic segment  $i$ , the two boundary conditions are given by imposing displacement and rotation continuity in correspondence of adjacency point between segments  $i - 1$  and  $i$ .

In this way it is possible to obtain a continuous elastic line that represents global variable section beam flexural behaviour.

### **Algorithm**

The model is implemented using Wolfram Mathematica.

First of all Young's modulus and load condition (tip force or distributed load) are set, together with every possible segment length and cross section moment of area. Surfaces are slightly simplified such that all section moments can be described by only three geometrical parameters:

$a$  : external tube diameter

$b$  : internal rod diameter

$c$  : flexures width, vertical dimension of most compliant sections

In this way one can obtain different geometries only by varying these three values.

Here follows the list of all section moments, from figure 4.5, where light blue parts represent the inner rod, and grey parts represent the outer tube, considered together as a single body. In figure 4.6 it is showed where these sections are located in a sliding segments beam sample.

- 1) Full circular section of inner rod, outer tube not present.

$$J_1 = \pi \frac{b^4}{64}$$

- 2) Stiffest case in which the two part form a full circular cross section.

$$J_2 = \pi \frac{a^4}{64}$$

- 3) Most compliant section, that occurs when rod and tube flexures are aligned both axially and angularly.

$$J_3 = \frac{ac^3}{12}$$

- 4) Stiffer section that replaces **3** when rod is fully shifted in axial direction.

$$J_4 = \pi \frac{b^4}{64} + \frac{(a-b)c^3}{12}$$

- 5) Section that replace **2** when inner rod is fully shifted in axial direction.

$$J_5 = \pi \frac{a^4 - b^4}{64} + \frac{bc^3}{12}$$

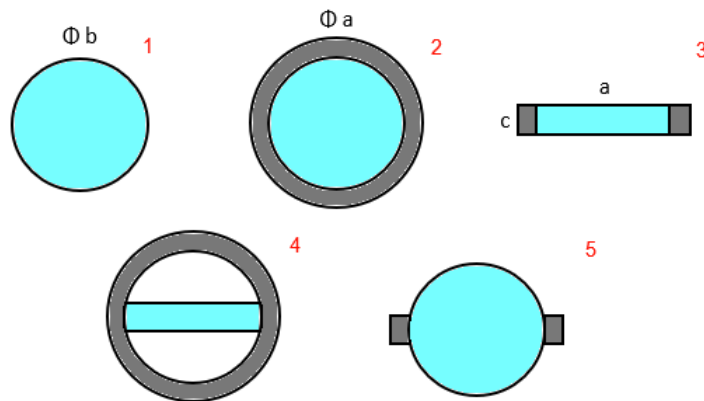
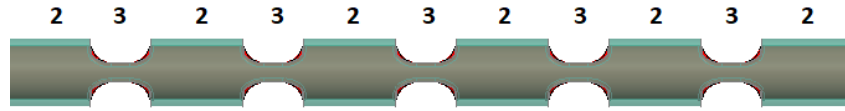
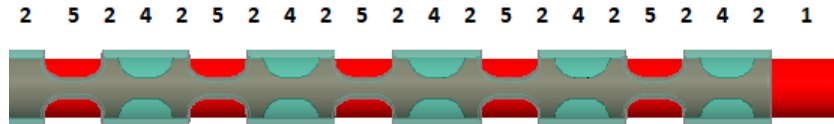


Figure 4.5: Possible simplified sections in sliding segments model



(a) unshifted



(b) shifted

Figure 4.6: Locations of listed sections of fig. 4.5 in sliding segments sample

Various configurations achievable through these sections are discussed in the following chapter. Then bending moment equation is written as function of  $x$ , given the applied tip force  $F$  and total beam length  $L$ .

$$M(x) = -xF + FL \quad (4.3)$$

At this point beam equations are written.

One has to note that each configuration has in general a different number of segments showing the aforementioned section properties. This corresponds to a different number of equations and boundary conditions, indeed a system of ODE is written for each configuration achievable with a single geometry. Let's say  $n$  is the number of segments forming a certain configuration and  $l$  values represent incremental lengths (e.g.  $l_2$  is the sum of first and second segments lengths). The generic  $I_i$  value is equal to one of the moment of area described above (see fig. 4.5 and 4.6).

Hence the system takes the form:

$$\left\{ \begin{array}{l} v_1''(x) = \frac{M(x)}{EI_1} \\ v_2''(x) = \frac{M(x)}{EI_2} \\ \dots \\ v_n''(x) = \frac{M(x)}{EI_n} \\ \\ v_1(0) = 0 \\ v_1'(0) = 0 \\ v_2(l_1) = v_1(l_1) \\ v_2'(l_1) = v_1'(l_1) \\ \dots \\ v_n(l_{n-1}) = v_{n-1}(l_{n-1}) \\ v_n'(l_{n-1}) = v_{n-1}'(l_{n-1}) \end{array} \right. \quad (4.4)$$

Once the system is integrated, one can show the elastic line as a continuous global function. The single end point vertical displacement is sufficient to evaluate an equivalent beam stiffness, which is considered for tested samples as ratio between tip force and correspondent displacement. An example is showed in fig. 4.7: 250 mm steel beam with tube diameter  $a = 6$  mm, rod diameter  $b = 5$  mm, flexure width  $c = 2$  mm, distributed load of 0.02 N/mm. Furthermore, it is possible to insert in this model beam segments composed by different materials, if one is much more softer than the other one. In this case, for sections where both materials are present, the soft part is neglected (for each section only a single value of  $E$  can be defined).

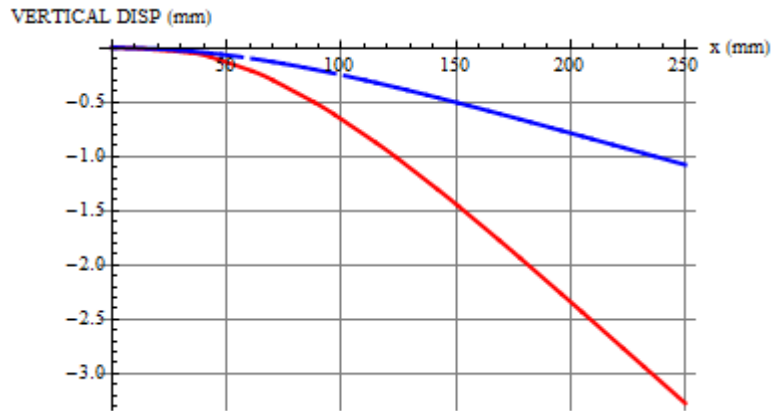


Figure 4.7: Elastic lines derived by solving analytic beam model: fully shifted configuration in blue, unshifted configuration in red

## 4.2 Rotary spar

The second investigated concept is a beam-like component capable to change its flexural stiffness via rotary movement. It can be seen as an improvement of a simple beam with discrete rotational symmetry.

This solution is strictly connected with sliding segments stiffening concept showed in the previous section.

The concept is based on pure component rotation: a beam with non axial-symmetric section changes its bending stiffness in vertical direction when it is rotated around its axis, because of the different material distribution around the cross section horizontal axis and the different orientation of central inertia axes.

### 4.2.1 Rotary rectangular beam

A rectangular  $a \times b$  section beam is taken as example, with  $a > b$  (fig. 4.8). The beam is constrained in cantilever configuration, with fixed-free ends. Considering a plane perpendicular to beam axis and a reference frame attached to the beam, with origin in the section geometric center, let  $x$  and  $y$

represent the section central inertia axes, and  $I_x$ ,  $I_y$  relative principal moments of area, given by

$$I_x = \frac{ab^3}{12} \quad I_y = \frac{ba^3}{12} \quad (4.5)$$

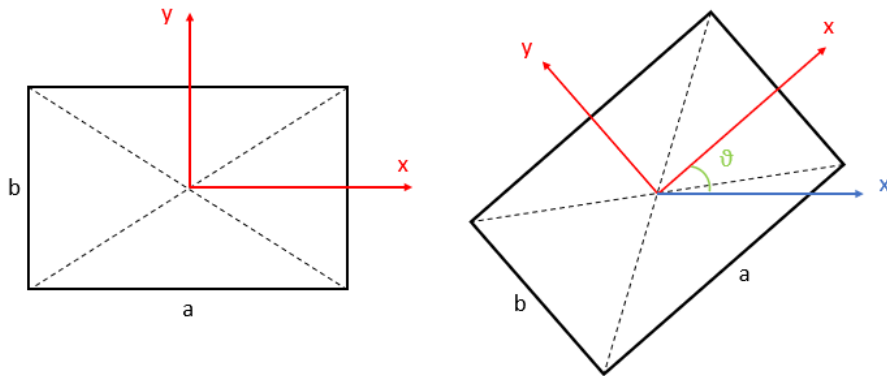


Figure 4.8: Rectangular section rotation

Bending stiffness of the beam depends on second moment of area relative to horizontal axis, material Young's modulus, beam length, and it's given by different formulas depending on load type and boundary conditions. By rotating the beam around its axis of an angle  $\theta$  (positive counter-clockwise) all mentioned parameters stay fixed except for the section moment of area. Let  $x'$  be the new horizontal axis after the section rotates (fig. 4.8).

The most compliant configuration is given when the rectangle lies horizontally:  $\theta = 0^\circ$ ,  $x' = x$ . The stiffest configuration is given when the rectangle lies vertically:  $\theta = 90^\circ$ ,  $x' = y$ . These two configurations are particular, since vertical bending stiffness is evaluated using a principal section axis. This problem, called "simple bending", is solved via classic beam theory such as Euler-Bernoulli beam theory (see section 4.1.3).

For  $0^\circ < \theta < 90^\circ$  horizontal axis is no more principal. In this case vertical

bending moment is split into two components along principal axes and two simple bending problems are solved. Superposition principle is then applied to derive beam stresses and displacements. Moment component along  $x$  generates beam bending along  $y$  direction, while component along  $y$  generates deflection along  $x$  direction.

For instance, in case of  $\theta = 45^\circ$  the bending moment is split into two identical components along  $x$  and  $y$ , but, since  $a > b$  and  $I_x, I_y$  depend on  $b^3$  and  $a^3$  respectively, displacement components due to bending along  $x$  and  $y$  are different: beam is much more compliant along direction which correspond to the smaller edge, i.e.  $y$  (fig. 4.9). For this reason, when a vertical bending load is applied, the beam bends along a preferred direction, with a non negligible horizontal component.

This implies that a simple rectangular rotary beam can only work as a dual stiffness solution: for  $0^\circ < \theta < 90^\circ$  beam shows displacements or forces in unwanted directions, denying possible in-between states with intermediate stiffness values in vertical direction.

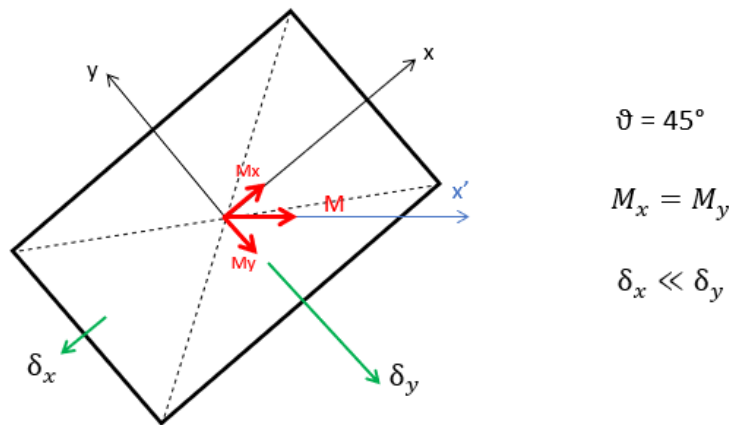


Figure 4.9: Example of bending along a non principal inertia axis

### 4.2.2 Improvement

The problem can be solved by modifying the section such that central axes lie as much as possible in horizontal and vertical directions for each value of  $\theta$ . By constraining unwanted horizontal deflections it would be possible to obtain a variable stiffness rotary spar working also with intermediate states. One way to reach this objective is to add to the section a portion of material which does not rotate, such that it shows an elastic compliant behaviour in vertical direction, while being rigid along perpendicular direction.

Such behaviour is per definition typical for a flexure (see 4.1.2).

Thus, this additional material should represent an obstacle to the horizontal displacement component generated by inclined rectangular section beam, when subjected to bending loads.

Like shown in the example of figure 4.10, where  $\theta$  is the angle representing rectangular section rotation around beam axis, and  $\alpha$  is the angle between central inertia axis  $x$  and horizontal axis  $x'$ , with this type of cross section and a  $45^\circ$  rotation it is possible to reduce  $\alpha$  of about two-thirds, with a consequent reduction of horizontal bending.

Obviously this implies a beam-like element, like in previous sliding segments concept, made of two separate bodies, internal and external.

Rounded geometry of fig. 4.10 is no coincidence: it is substantially a cross section of a sliding segments sample described in section 4.1, taken in unshifted configuration, in correspondence with tube and rod flexures. The only difference is that inner rod is rotated. Such degree of freedom is not denied for the sample.

In principle the outer body can be thought as a single long flexure, but it would be too fragile for any applications. Tubular segments alternated with lumped compliances can be suitable for this solution.

About the inner body, it could be a thin rectangular beam, but in such case torsional effects would be significant, especially due to friction forces exchanged with outer tube during rotations. A geometry in which rectangular segments alternate with full circular sectioned parts represents a good compromise.

Therefore it is shown that a specimen created as sliding segments variable stiffness beam can be also suitable for this second solution. Tests and results are described in following sections.

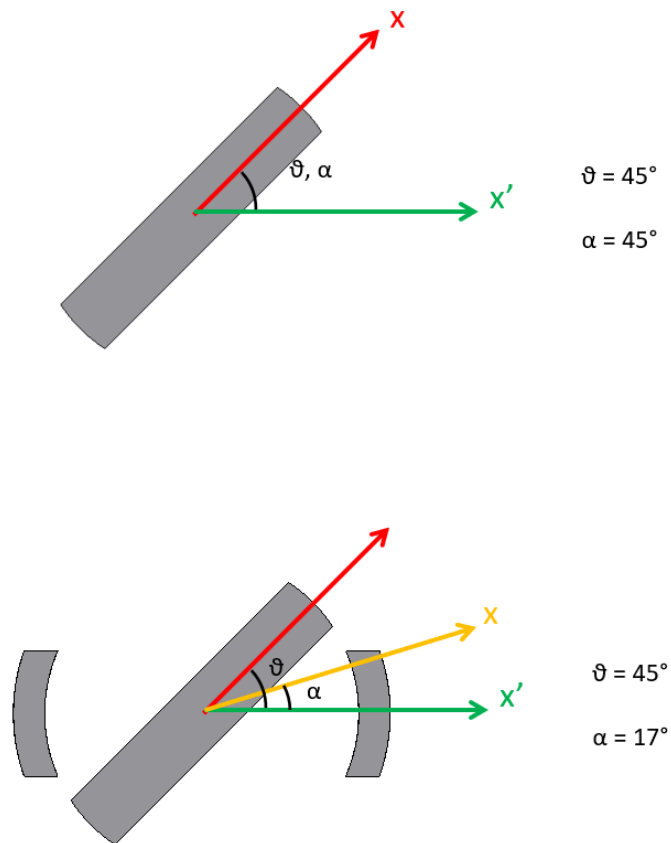


Figure 4.10: Example of  $\alpha$  reduction due to additional material

# Chapter 5

## Methodology

In this chapter the fabrication of multiple specimens is described, as well as the building of a set-up to characterize the bending stiffness of beam-like elements in cantilever configuration.

### 5.1 Specimens fabrication

Three different specimens are fabricated: two of them can be tested both as sliding segments beams and rotary spars, while one can only be used to test the first concept, due to its axial-symmetric geometry.

#### 5.1.1 Onyx sample

After some attempts, a first prototype is 3D printed with Markforged Mark Two printer, with thickness of each layer of 0.4 mm and using Onyx filament: a composite material made of nylon and chopped carbon fiber, offering smooth surfaces and maintaining resistance and flexibility features (fig. 5.2). These characteristics allow the specimen to undergo several tests and huge clamping forces without breaking. Rod and tube are printed vertically, with the disadvantage of possible delamination of the printed layers: a previous attempt to print them horizontally ended up in fragile components with rougher surfaces.

In this case flexures rely on smaller cross section second moment of area to achieve compliance.

## Geometrical properties

In this paragraph the main geometrical properties characterizing the sample are defined.

Like in previous section nomenclature, tube diameter, rod diameter and flexure vertical dimension are indicated by  $a$ ,  $b$  and  $c$ , respectively. Other significant parameters are given by  $L$  and  $l$ , which define respectively rigid segment and compliant flexure lengths. From these two dimensions one can evaluate sample aspect ratio, defined as  $AR = \frac{l}{L}$ , the amount of shift  $sh = \frac{L+l}{2}$  between the two limit configurations, and length of parts where rod and tube rigid segments are overlapped in fully shifted state, namely  $ov_{fs} = \frac{L-l}{2}$ .

The last two mentioned characteristics are only significant when the sample is tested as sliding segments variable stiffness beam. All geometrical parameters are explained graphically in fig. 5.1 and values are shown in table 5.1.

$a$ (mm)	$b$ (mm)	$c$ (mm)	$L$ (mm)	$l$ (mm)	$AR$	$sh$ (mm)	$ov_{fs}$ (mm)
11	9	3	20	10	0.50	15	5

Table 5.1: Geometrical properties for Onyx prototype

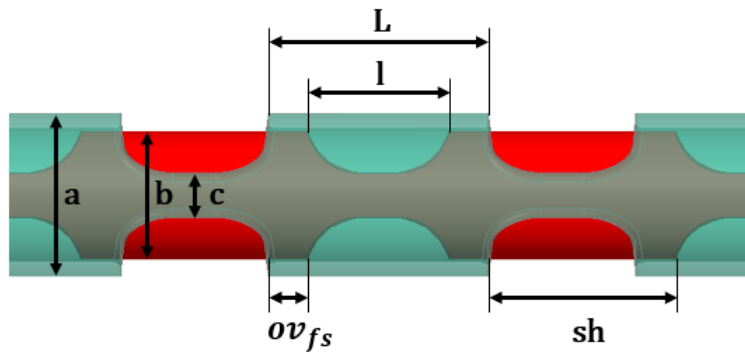


Figure 5.1: Geometrical parameters describing the built samples



Figure 5.2: Onyx sample: inner and outer parts, unshifted configuration, fully shifted configuration

### 5.1.2 Aluminium sample

The second prototype is manufactured of aluminium alloy (fig. 5.4). A good fit between rod and tube allow them to be milled at the same time, while being one inside the other. Relative position is fixed by means of a pin, and two plastic supports are cut in order to properly clamp the beam in the milling machine. Manufacturing set-up is shown in figure 5.3.

Like for previous specimen, flexures are obtained by changing beam geometrical properties. The main differences with respect to Onyx sample are that

it is made of a solid material, not 3D printed, geometry is more accurate, there is less play between rod and tube, it shows smaller aspect ratio and bigger “overlapping” (tab. 5.2), it is globally stiffer and it does not have delamination problems due to printing.

### Geometrical properties

$a$ (mm)	$b$ (mm)	$c$ (mm)	$L$ (mm)	$l$ (mm)	$AR$	$sh$ (mm)	$ov_{fs}$ (mm)
8	6	1.6	26	10	0.38	18	8

Table 5.2: Geometrical properties for aluminium prototype



Figure 5.3: Aluminium sample manufacturing

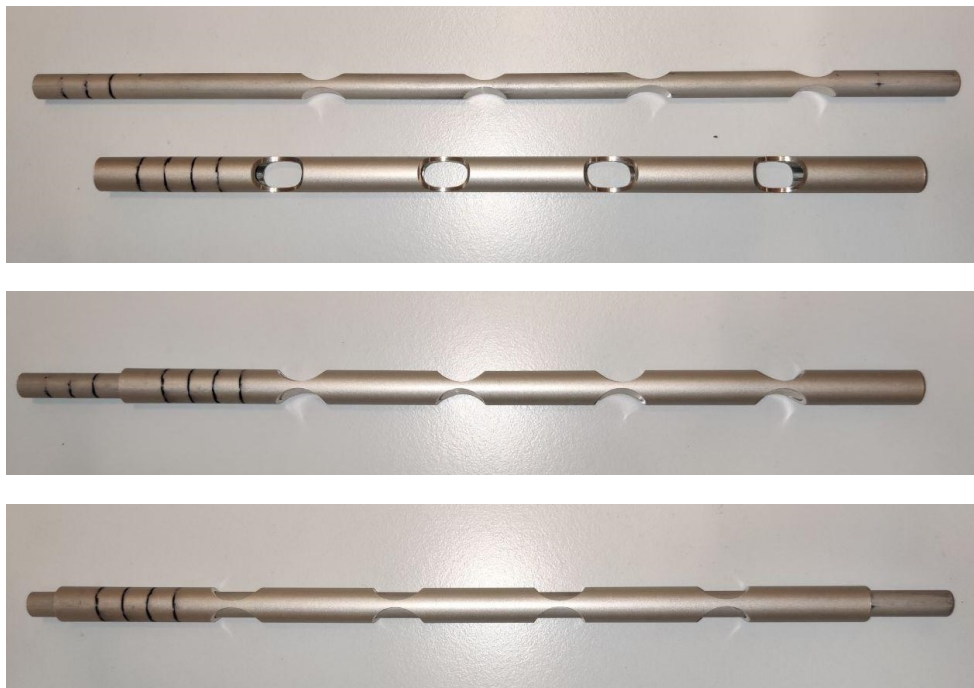


Figure 5.4: Aluminium sample: inner and outer parts, unshifted configuration, fully shifted configuration

### 5.1.3 Multi-material sample

The third prototype is different from previous ones: it shows an axial-symmetric geometry: flexures compliance is achieved by only changing material elastic properties (fig. 5.5). For this reason here  $c$  is not defined.

Sample is 3D printed with Stratasys Objet260 Connex3 printer using PolyJet technology, capable to work with multiple materials and to achieve high quality prints. PolyJet is a 3D printing technology that builds parts by jetting thousands of photopolymer droplets onto a build platform and solidifying them with a UV light. It's one of the fastest and most accurate 3D printing technologies currently available [45]. The printer works with a rigid and a soft material simultaneously: users can set the percentage of each material to obtain desired properties. In this case Vero White and Vero Clear, most rigid available materials showing equivalent elastic modulus of 3 Gpa, are chosen for tube and rod segments, respectively. The second one

is transparent, allowing to see the inner sections. Agilus Black, rubber-like material, with  $E = 4$  MPa (approximated from its shore stiffness), is used to print flexures. By changing material properties, the flexural stiffness ratio between compliant and rigid parts is way bigger than the one achievable by only change geometric properties without making the beam too fragile. This prototype shows also the lowest aspect ratio and the biggest “overlapping” values (tab. 5.3), compared to previous samples.

### Geometrical properties

$a$ (mm)	$b$ (mm)	$L$ (mm)	$l$ (mm)	$AR$	$sh$ (mm)	$ov_{fs}$ (mm)
12	9	25	7	0.28	16	9

Table 5.3: Geometrical properties for multi-material prototype

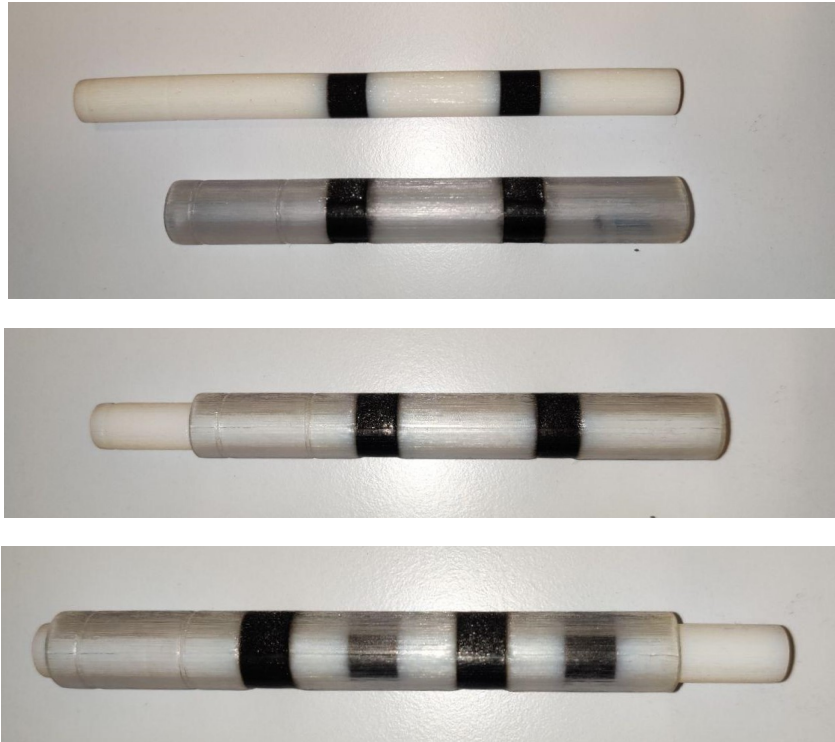


Figure 5.5: Multi-material sample: inner and outer parts, unshifted configuration, fully shifted configuration

## 5.2 Experimental set-up

In the following experiments samples are subjected to bending thanks to a SMAC LCA25-050-15F moving coil linear actuator (fig. 5.6) which end effector is controllable either in force or displacement, while the other variable is measured [46]. This actuator offers a maximum stroke of 50 mm with a maximum force of 15 N (peak) or 6 N (constant). Force and displacement values are evaluated according to the last actuator calibration.

Sample is constrained in cantilever configuration, with fixed-free ends and tip concentrated load. A certain amount of vertical displacement is imposed at beam tip, in a one-directional way, while beam root is constrained by a bench clamp. Position control script is implemented in Matlab. The reaction force signal from beam to actuator is then acquired. Samples bending stiffness is evaluated by dividing measured beam tip force value by correspondent displacement (quick scheme in fig. 5.7).

Measurements are repeated for each samples' configuration, i.e. with different relative position or orientation between the inner rod and the outer tube, with the beam clamped such that its length stays constant. Experimental set-up is shown in figure 5.8.

Geometry of each sample tested as sliding segments beam is such that bending moment vector always lies in a central inertia plane, so deflections and forces stay in desired direction. Experiments are carried out making sure to always remain in elastic region for all specimens, avoiding permanent bending.

With this kind of actuator it is possible to impose continuous displacements in order to construct continuous force-displacements curves. A quasi-static approach is in this case preferred, because of some factors influencing force signal in the continuous case:

- Inertia forces on end effector
- Actuator internal friction
- Noise

An approach to construct discrete force-displacement curves is indeed chosen. Displacements are imposed by multiple steps of 2 mm each, with 5 s intervals

between one step and the following one. These time intervals allow the force to reach “steady state” values for polymeric samples and, moreover, allow to add more signal points to averages and therefore to get more reliable measurements. About polymeric samples, non constant deformations are expected for constant forces, because of their viscoelastic nature.

### Measured displacements

Measured displacements are in this case very accurate and precise, oscillations with respect to imposed values are of  $10^{-3}$  mm order of magnitude. For this reason there is no need to perform signal processing or error analysis, indeed end effector real displacements are considered coincident with imposed ones (fig. 5.9). Small oscillations only occur near to almost instantaneous position jumps.

### Measured forces

With used actuator measured forces are quite noisy: for each step of displacement, correspondent force is evaluated by averaging “steady state” signal values. Force values correspondent to jumps between different actuator positions are not included in averages, as well as initial decreasing force values due to viscoelastic effects in polymers. Then standard deviation is calculated to show values distribution around the mean, to add accuracy information to each force point, plotted in a force-displacement discrete curve. Examples in fig. 5.9.



Figure 5.6: SMAC LCA25-050-15F linear actuator used for bending tests

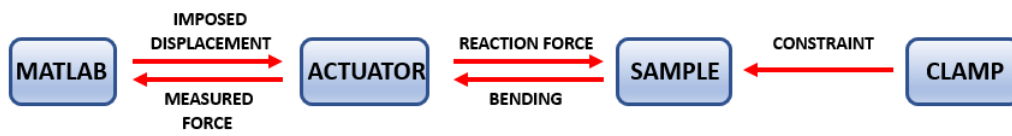


Figure 5.7: Scheme of the built set-up to perform bending tests for beam elements

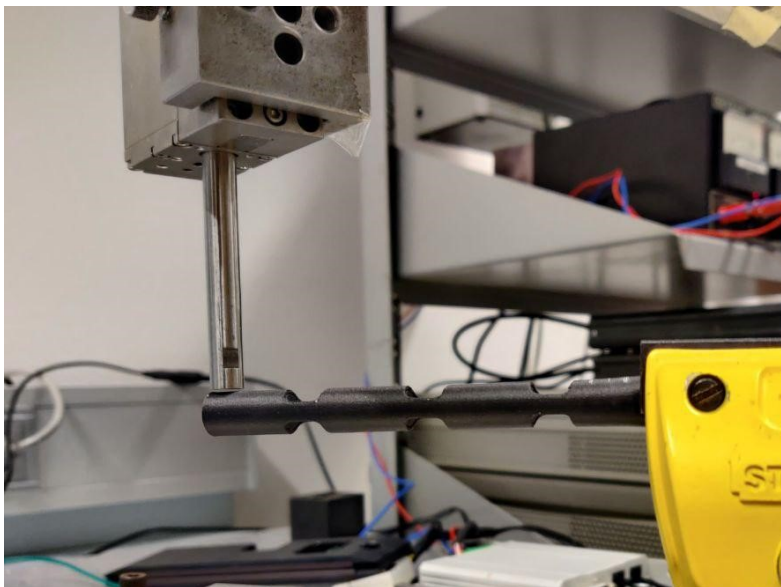
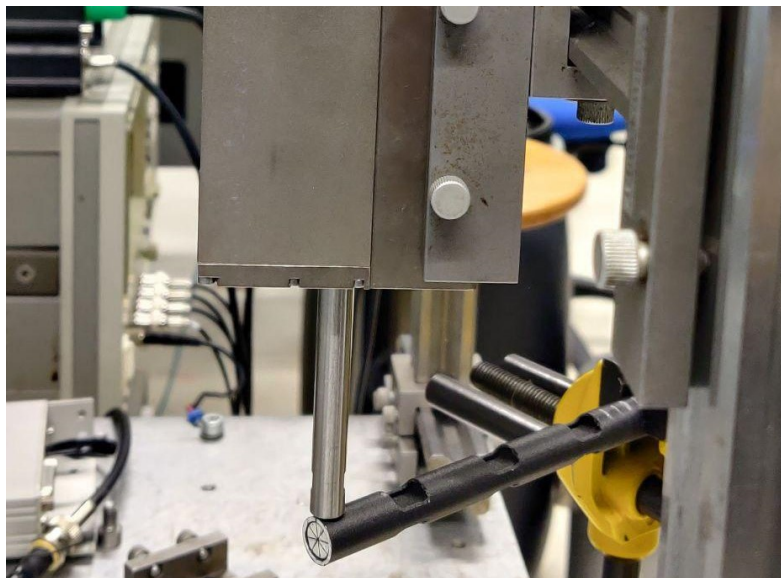


Figure 5.8: Experimental set-up to derive flexural stiffness of beam-like elements subjected to bending

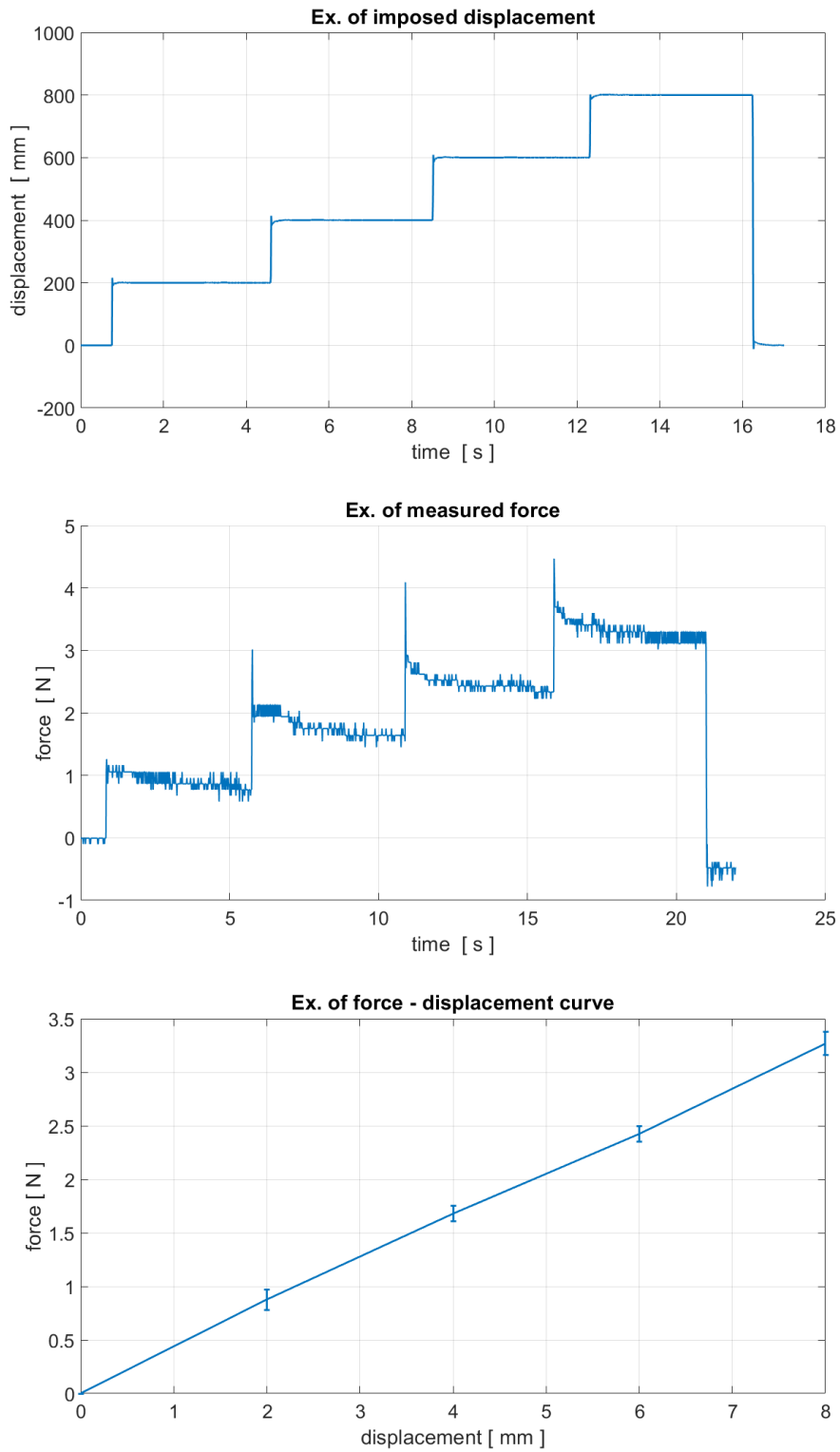


Figure 5.9: Examples of measured displacement, measured force, force-displacement curves with error analysis, relative to multi-material sample bending test

# Chapter 6

## Results & Discussion

In this chapter the results and analysis from bending tests are shown for all specimens and for both concepts: sliding segments beam and rotary spar. Achieved results are then discussed.

### 6.1 Sliding segments

In this experiments samples' configurations are given by different relative position between rod and tube, with fixed orientation.

Each configuration corresponds to a bending measurement. Sliding segments is abbreviated as "SS" in plots titles.

#### 6.1.1 Onyx sample

Results are derived from force-displacements curves shown in figure 6.1. Curves correspondent to four configurations (unshifted, 5, 10, 15 mm shift) are slightly different from each other, and an approximately linear trend is showed. Large standard deviation values given by accuracy analysis make these differences meaningless. Therefore curves could be considered overlapping. This would mean that Onyx sample does not stiffen by shifting the inner part, and that the studied principle does not work in this case: force displacement curve is the same despite shifting. Actually it is difficult to derive a final conclusion about this specimen. Reason of that is in low compatibility between flexible samples and available instrumentation. Main disadvantage

of specimen made of compliant material is that force differences in  $y$  axis are small, and systematic inaccuracies given by the instrument have more weight with respect to an experiment with a stiffer sample, given the same amount of displacement. The measured accuracy, as one can see from vertical bars in force-displacement curved, is in general approximately  $\pm 0.05$  N, and behaviour of such compliant sample may not be caught properly with the used linear actuator. These results are not comparable with analytic model because the huge difference in filling methods used to print inner and outer parts leads to different material properties, therefore an equivalent Young's modulus cannot be estimated for this sample.

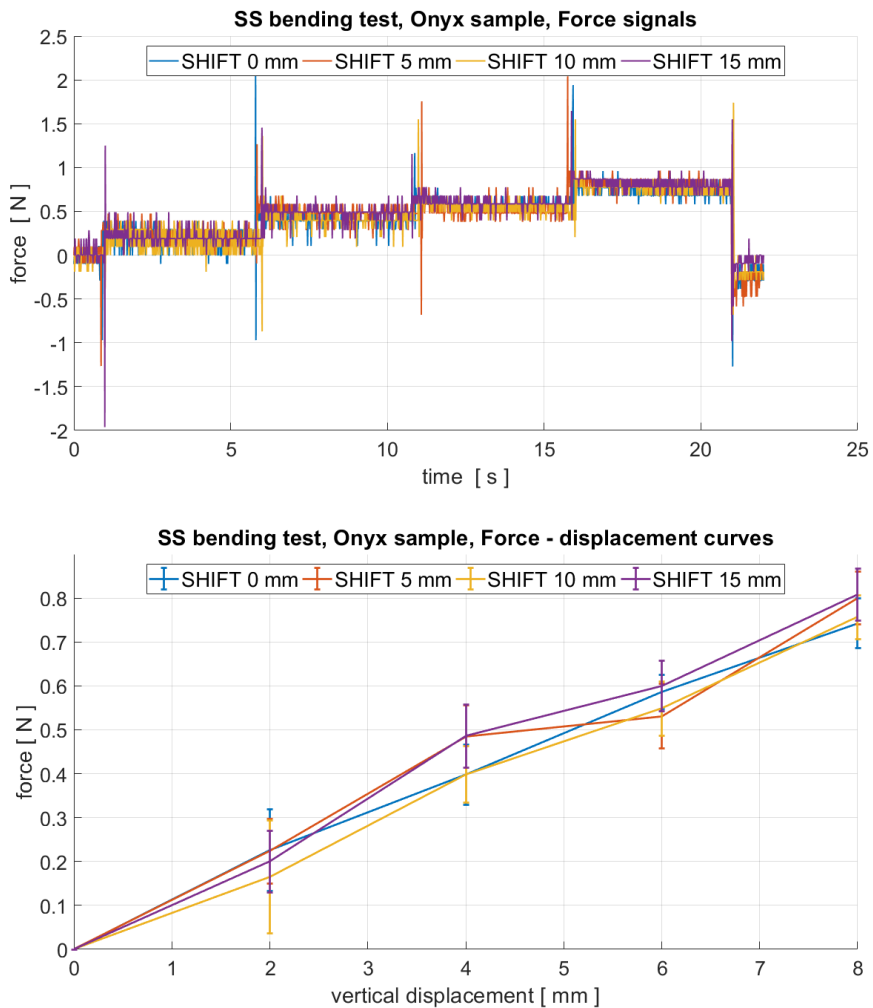


Figure 6.1: Bending tests results for Onyx prototype as sliding segments beam

### 6.1.2 Aluminium sample

Results from the experiment with aluminium sample are shown in fig. 6.2. Trends are in general quite linear, with a slightly decreasing slope for biggest loads.

From these results, one can see a small but clear increasing difference in force values between the red and yellow curves, respectively correspondent to unshifted and fully shifted configuration. Slope difference implies stiffness difference. This occurs when vertical beam tip displacement becomes bigger than 4 mm. In fact, after this threshold, considering accuracy given by standard deviation values, the two curves can be seen as not overlapped, with stiffer fully shifted state. One can also state that stiffening occurs below 4 mm, but with some level of uncertainty.

Similar consideration can be made for the two intermediate states, but displacement threshold is in this case bigger, namely 8 mm. The two curves can be considered overlapped and between the two limit states before displacement reaches this value. After 8 mm blue and purple curves separate and they reach force values similar to the two limit configurations.

With this specimen it is possible to better catch differences between its configurations: solid and stiff material allow measurements to be more precise, due to the smaller weight of instrumentation inaccuracies.

It is then possible to state that sort of expected stiffening is shown by this sample, albeit in a small measure: stiffness ratio  $SR$ , namely the ratio between most rigid and most compliant states, keeps a constant mean value of  $SR = 1.1 \pm 0.1$ , since when the two curves can be considered as separated from each other. In this range, stiffness ratio does not change by increasing the load, even though it is quite small. This behaviour also demonstrate the linear trend of unshifted and fully shifted force-displacement curves in this range.

Geometry of this sample is inserted in single elastic linear beam model, which does not represent well the reality. Further discussion is found in section 6.1.4.

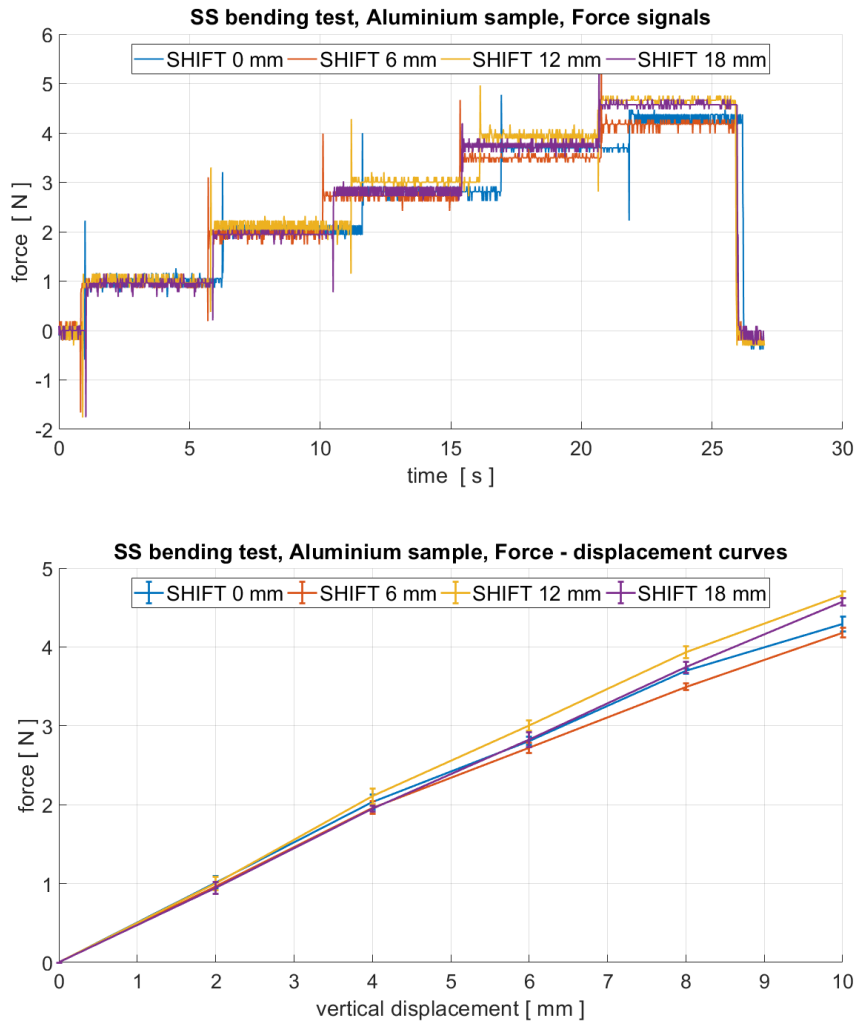


Figure 6.2: Bending tests results for Aluminium prototype as sliding segments beam

### 6.1.3 Multi-material sample

Results achieved by multi-material prototype bending tests are shown in plots of figures 6.3 and 6.4.

Also in this experiment trends of force-displacement curve are roughly linear. Stiffening by shifting inner rod does occur in a large way for this sample, allowing also results to be more accurate, thanks to bigger differences in force values.

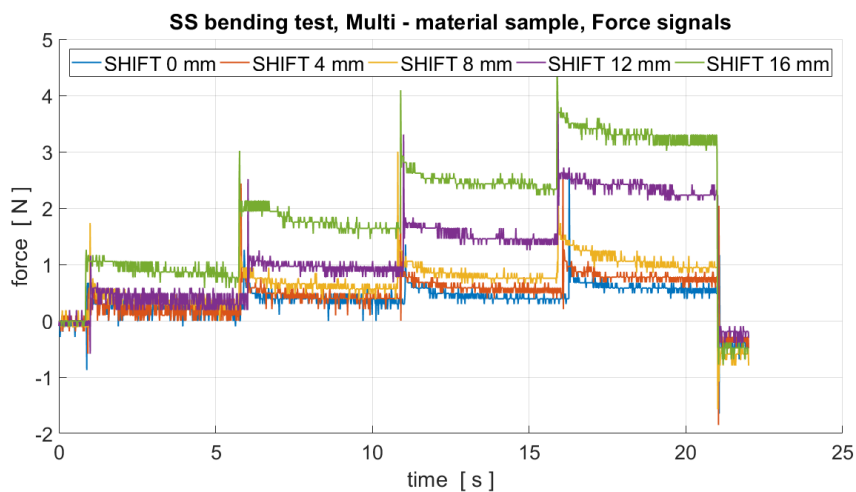
For in-between states, from 6 mm onwards stiffening clearly occurs, since in

relative plots errors do not overlap any more.

In first plots every curve represents a constant shifting value: all configurations behaviour by increasing tip load is showed. In 6.4 curves are characterized by constant vertical displacement: every plot shows what occurs by shifting the inner rod for different displacement and load values. Passing from force to stiffness plot, uncertainty values are kept constant in percentage. Propagation of errors is applied, considering as exact displacement values. This is reasonable as shown in section 5.2, paragraph “Measured displacements”. Since measured error is systematic, its percentage is bigger for lower force values. For this reason the uncertainty in the measurements with 2 mm displacement (blue curve) is bigger. Stiffness ratio is derived from fig. 6.4 by averaging stiffness values relative to 0 mm and 16 mm shifting, and excluding the most uncertain one. Propagation of errors is applied.

$$SR = 5.2 \pm 3.1$$

Differences in slope between force-displacement curves relative to different configurations vary with a trend that shows increasing positive slope, with smaller gaps between first three states (unshifted, 4 mm, 8 mm shift) and bigger gaps between other ones (12 mm, 16 mm shift). This trend, discussed in section 6.1.4, is clearly seen in stiffness-shifting curves, and it is quite the same for every imposed displacement.



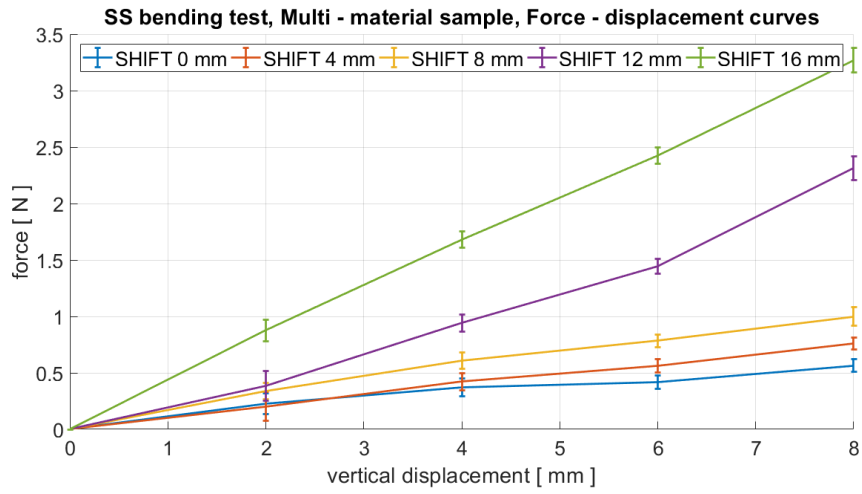


Figure 6.3: Bending tests results for multi-material prototype as sliding segments beam

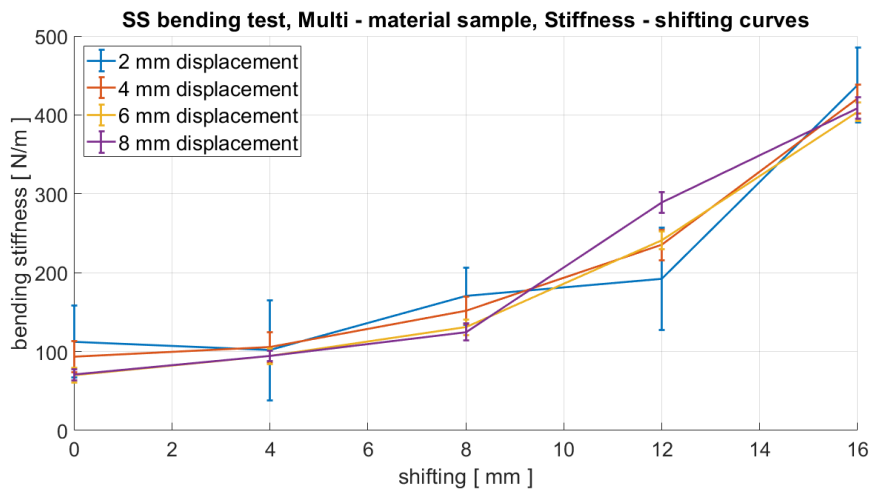


Figure 6.4: Multi-material prototype: stiffness-shifting curves

### 6.1.4 Discussion - Sliding segments

In this section results achieved by exposed experiments about sliding segments concept are discussed. Connections and motivations between successive steps are described.

#### Onyx sample

From the obtained results it would seem that the studied concept does not work at all for this first 3D printed prototype. Again, actually it is not possible to state any conclusions: beam flexural stiffness could change with small variations, not observable with used linear actuator and its accuracy level.

From here comes the necessity to build a different specimen, with the same working principle, but stiffer. In this way instrumentation accuracy has smaller weight on experimental results.

#### Aluminium sample

With this second stiffer prototype it is possible to note the predicted behaviour related to proposed concept, although only slightly.

Given plots in fig. 6.2, one can imagine that, by increasing the beam load even more, stiffening behaviour would be better noticed for limit configurations and middle states. Actually, in such case plastic deformations would occur soon, bending the sample in a permanent way.

Stiffness ratio  $SR = 1.1 \pm 0.1$  is very small and keeps a constant value by varying the load, even though, due to accuracy issues, it has been possible to evaluate it only for high loads. Since force-displacement curves are roughly linear, it would be reasonable to think that Euler-Bernoulli linear model can be suitable for this solution. Actually, by analytically modelling aluminium prototype the following results are obtained: in unshifted state bending increases with load in a certain way (very different from reality), while beam in fully shifted configuration is orders of magnitude stiffer. It is then possible to suppose that stiffening does not occur, like hypothesized in analytic model, because of pure cross sections properties without any kind of influence be-

tween rod and tube as separate bodies, and the most likely explanation in that the single elastic body hypothesis does not hold for this solution. In that case measured  $SR$  would have been much bigger.

It is more reasonable to say that beam stiffness changes especially because of the interaction between two bodies in contact.

From this hypothesis came the idea of building another specimen which highlights this aspect.

### **Multi-material sample**

To emphasize interactions between inner rod and outer tube one can choose to make the flexures more compliant and to decrease the aspect ratio  $AR$ , such that length  $ov$  of the overlapped rigid parts in shifted configurations is bigger. Importance of aspect ratio and overlapping is shown also in [34], where “sliding layer” concept is studied for laminate structures.

However, by decreasing  $AR$  flexures become shorter, and then stiffer, if they rely only on cross section reductions (these reductions show a lower limit caused by beam fragility). Therefore the two parameters to be modified are in contrast with each other.

One way to make short and very compliant flexures is to change material properties. This is how the idea to build a multi-material prototype came up.

An axial-symmetric geometry is chosen to avoid possible printing errors, but it does not represent a constraint for future studies: it is still possible to combine geometrical and material properties variations. Here rod and tube are indeed characterized by constant cross section.

To reach the compliance obtained thanks to Agilus Black material only with geometrical changes, flexures should be way longer.

If  $K_s$  and  $K_f$  represent segment and flexure stiffness, respectively, simulations on laminates from [34] suggest the importance of  $\frac{K_s}{K_f}$  to be as big as possible, to achieve more stiffening (fig. 6.5), and this approach suits well with the multi-material specimen.

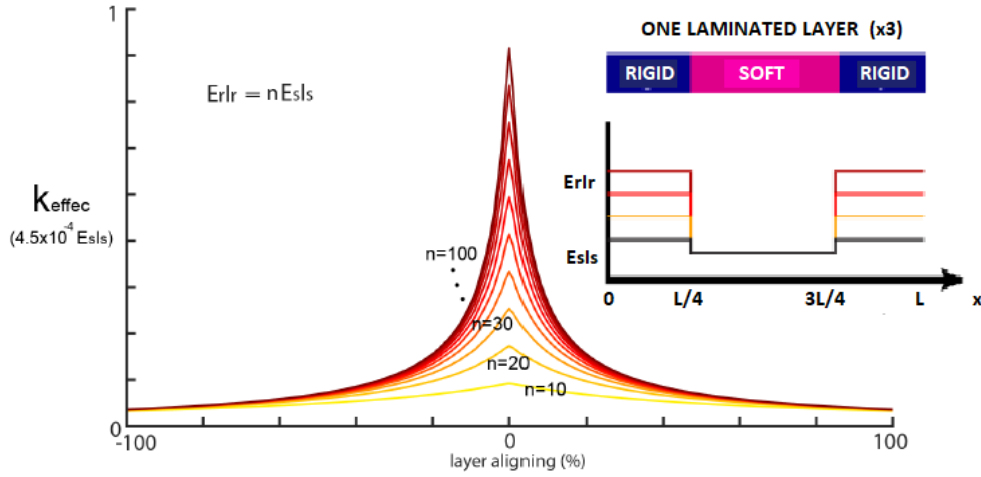


Figure 6.5: Simulations of sliding layer concept, with different stiffness of rigid parts:  $E_r I_r$  and  $E_s I_s$  are flexural stiffness of rigid and soft layers,  $n$  is their ratio,  $K_{effec}$  is global stiffness and  $L$  length of the laminate. From [34]

Results show that sliding segments concept works well with this prototype. Also this sample is modelled analytically, obtaining unrealistic results, like in the previous case.

The specimen shows a stiffness ratio  $SR = 5.2 \pm 3.1$ , giving a positive result. This happens due to the greater interaction between the two bodies, where the inner rod, when shifted, constraints the outer tube deformation.

When propagation of errors is applied for divisions, relative uncertainties are summed up, leading to a quite big uncertainty on  $SR$ , because of the  $\sim 40\%$  error on the most compliant state. This is again caused by the actuator used, affected by low resolution in force. This gives indications on how to improve experiments in future works.

By the way, the overlap  $ov$  represents a fundamental parameter, which assumes its maximum value  $ov_{fs}$  in fully shifted state and lower values elsewhere. Behaviour of not enough overlapped segments is highlighted in fig. 6.6: the inner part does not prevent the outer one to bend.

In this case, since flexure length is 7 mm and total shifting is 16 mm, divided in 4 steps of 4 mm each,  $ov$  assumes the following values:

- $ov_0 = 0$  mm
- $ov_4 = 0$  mm
- $ov_8 = 1$  mm
- $ov_{12} = 5$  mm
- $ov_{16} = ov_{fs} = 9$  mm

These values are strictly connected to the trend of stiffness-shifting plots in figure 6.4. These curves are really close to each other: this allow to suppose that stiffening is independent from the amount of imposed displacement, for small displacements.

It is then reasonable to average the points (and propagating the errors) to build a mean stiffness-shifting curve, shown in fig. 6.7. Slope of this curve is dual: at first it is positive but very small, since increasing shifting values do not correspond to increasing  $ov$  values. Slope rises up as relative overlapping values become positive.

It is then interesting to show how bending stiffness changes for positive values of  $ov$ . Figure 6.8 is an enlargement of fig. 6.7 in correspondence of positive  $ov$  values, placed in  $x$  axis. One can note that when shifting is such that  $ov$  become positive, then bending stiffness increases almost linearly with  $ov$ . Some important steps to characterize sliding segments stiffening mechanism are then achieved.



Figure 6.6: Example of not overlapped bended parts, from [34]

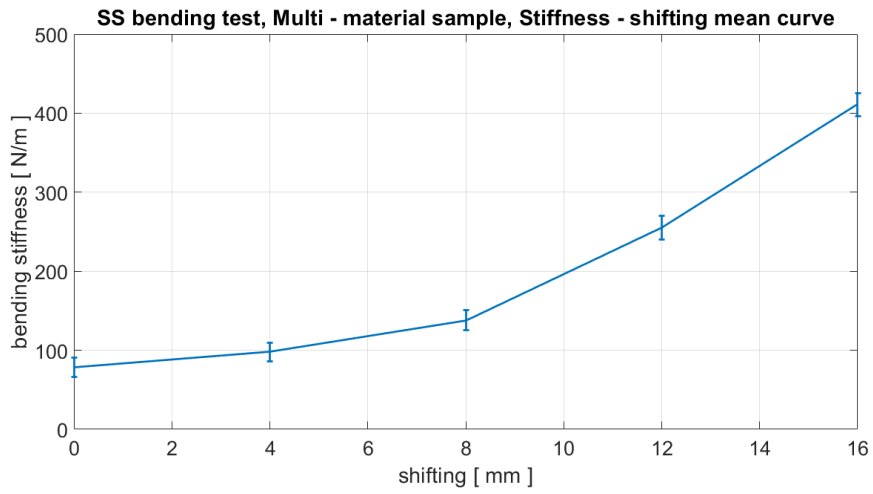


Figure 6.7: Multi-material prototype: stiffness-shifting mean curve

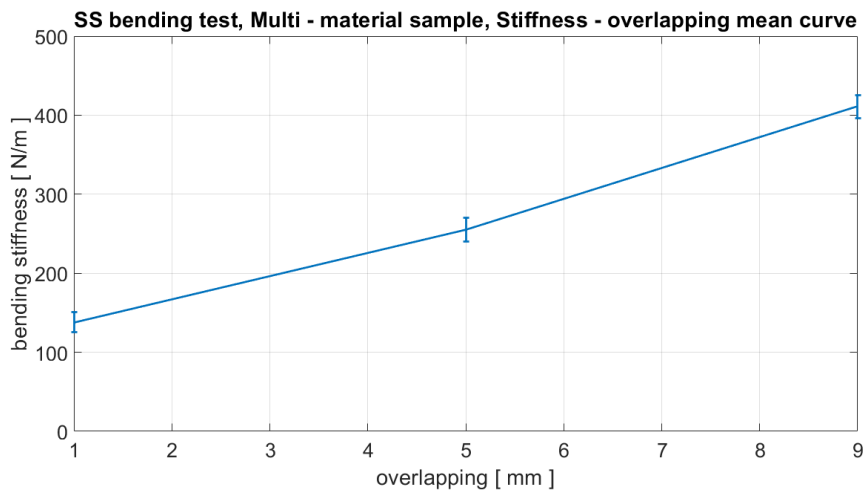


Figure 6.8: Multi-material prototype: stiffness-overlapping mean curve

## 6.2 Rotary spar

In this experiment sample configurations are represented by different orientations of the components. A rotation angle of the inner rod corresponds to a bending measurement.

The 3D printed prototype made of Onyx filament described in section 5.1.1 is chosen for this experiment despite the bigger uncertainties: the aluminium

sample (sec. 5.1.2) would be too stiff in vertical direction for  $\theta \simeq 90^\circ$ , thus reaction force on actuator end effector would risk to exceed the limit value of 6 N indicated in the manual for a constant force. The multi-material sample is not suitable because of its axial-symmetric geometry.

Error analysis is performed like in previous experiments of section 6.1. Rotary spar is abbreviated as “RS” in plots titles.

### 6.2.1 Rod

In the first test a rotary beam formed only by the internal rod of figure 5.2 is tested. The objective is to show consequences of deviated-bending and to compare results with the ones obtained with the discussed improved geometry (see paragraph 4.2.2).

Results are analysed from fig. 6.9 and 6.10.

Plotted points are affected by some uncertainty, especially when imposed displacement is 2 mm and measured force is low, because of aforementioned considerations.

Force-displacement curves show that the rod does not stiffen when rotated up to  $\theta = 45^\circ$ : like expected, a huge amount of horizontal bending occurs, leading to a small vertical reaction force value. For  $\theta = 67.5^\circ$  an intermediate stiffness value is obtained, but still with an unwanted horizontal displacement component. This is only avoided for  $\theta = 0^\circ$  and  $\theta = 90^\circ$ .

Also from stiffness-angle curves it is possible to notice that flexural stiffness in vertical direction only increases when  $\theta > 45^\circ$  and it is independent of imposed displacement. Curves relative to 2 mm and 4 mm displacement (blue and red in fig. 6.10) are slightly decreasing at first. This also could be due deviated bending: beam tip slides horizontally during the experiment, such that the beam axis is no more aligned with the actuator’s end effector. Reactions on the latter are then a force and a torque, which is not measurable. This can explain the low equivalent stiffness values.

This specimen confirmed a simple rotary beam to be a dual stiffness solution in practice, because of the horizontal displacement. In this case measured stiffness ratio between limit states is  $SR = 2.6 \pm 0.8$ .

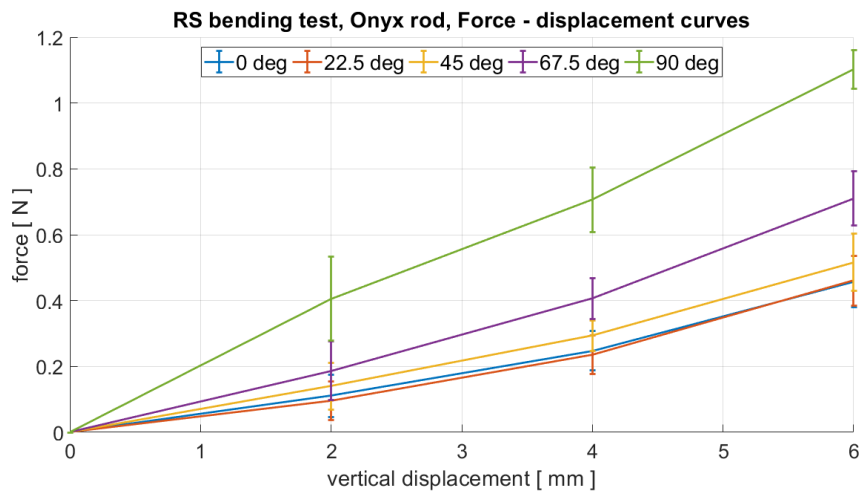
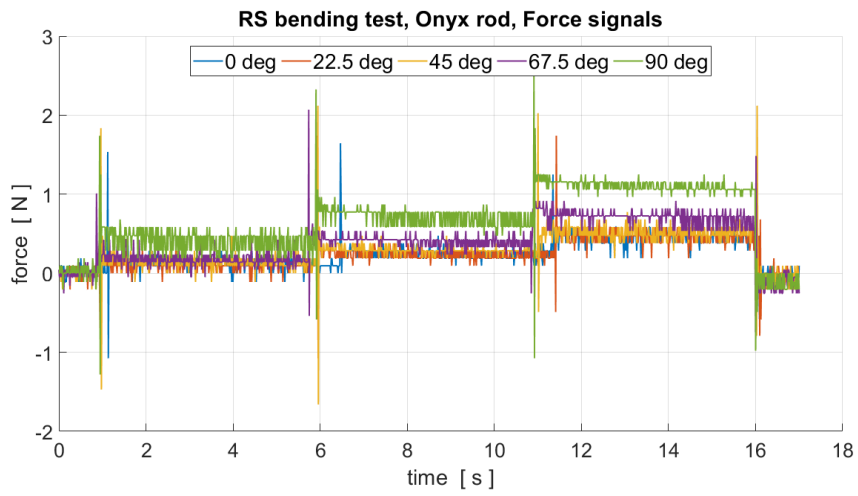


Figure 6.9: Bending tests results for Onyx rod as rotary spar

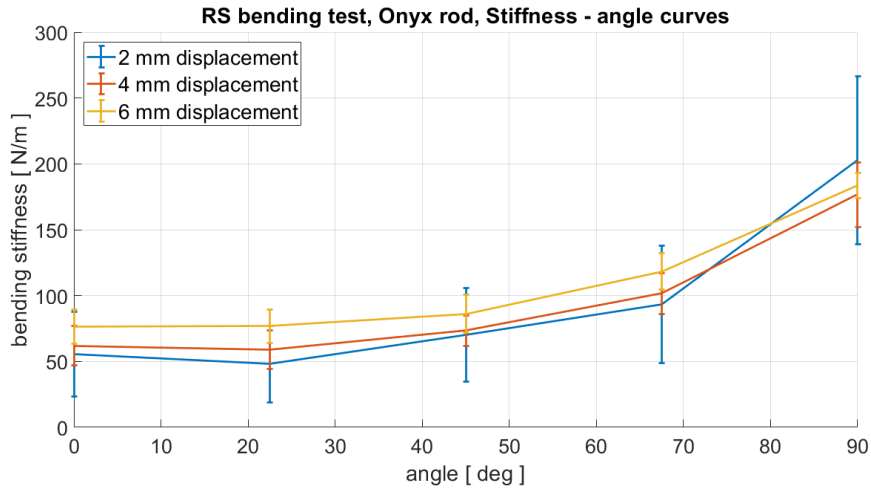


Figure 6.10: Onyx rotary rod: stiffness-angle curves

## 6.2.2 Rod plus tube

In this second test Onyx prototype is subjected to bending as rotary spar. With respect to the previous test, the outer tube is added, kept fixed, such that it is compliant in vertical direction and rigid in horizontal direction. Multiple configurations are given by different rod orientations.

Test shows that by adding stiffness in horizontal direction unwanted bending is avoided: there is no visible horizontal displacement in any configuration. Of course central inertia axes are still inclined and this problem is still classified as deviated-bending, but in a minor way.

Plots of figure 6.11 show that intermediate stiffness values are obtainable with this sample: force-displacement curves are clearly separate also for  $\theta \leq 45^\circ$ . In fact, stiffness-angle curves (fig. 6.12), compared with the previous test, are characterized by monotonous increasing trend. Like in the rod test, blue curve relative to 2 mm displacement is the most uncertain. Also in this case equivalent stiffness is showed to be independent of imposed displacement, for small displacements.

Measured stiffness ratio is  $SR = 2.1 \pm 0.6$ .

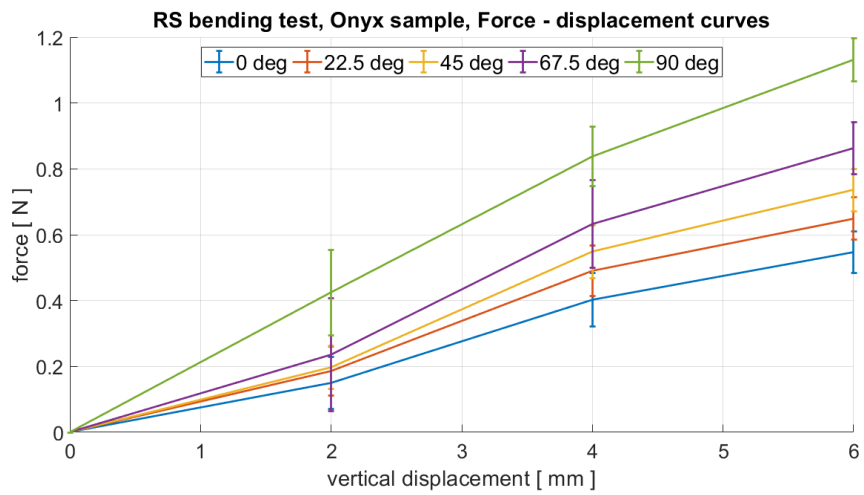
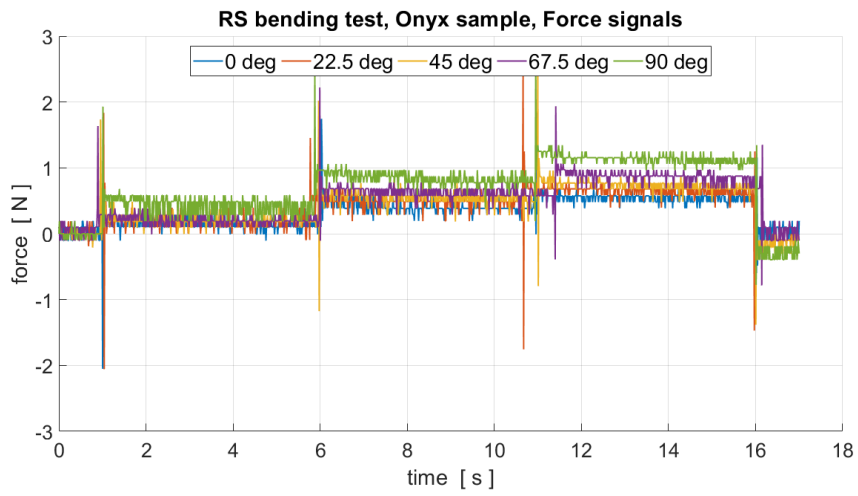


Figure 6.11: Bending tests results for Onyx prototype as rotary spar

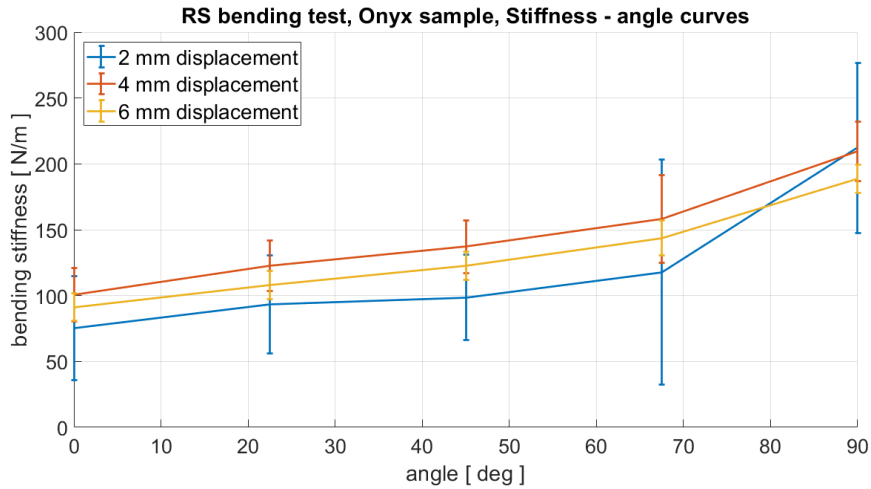


Figure 6.12: Onyx rotary spar, rod + tube: stiffness-angle curves

### 6.2.3 Discussion - Rotary spar

Results reveal that the improved geometry allows to have a rotary spar with multiple stiffness levels.

There is a compromise: by adding the outer tube central inertia axes inclination decreases, but also achievable stiffness range. In this case  $SR$  is decreased by 19% with respect to the dual stiffness solution. This decreasing is due to the additional tube, which does not contribute to the stiffness change.

Stiffness ratio values are not crucial in this step, they can be enlarged by changing sample geometrical parameters like  $AR$  and  $c$ .

One has to notice that these positive results are obtained with a sample that has been designed for sliding segment tests, exhibiting a suitable, but not optimized geometry to test the concept.

It is possible to suppose that for the rotary spar solution the single elastic body assumption holds better than for sliding segments: adding the outer tube is like adding a fixed quantity of horizontal bending stiffness to the inner rod. The overall sample can be studied as one single body for each of its configurations.

# Chapter 7

## Conclusions and future work

This study tries to answer the research question related to the Portwings project: “What are the best concepts and techniques targeted to implement variable stiffness in a flapping wing, especially as part of a smart wing spar?” From the comparison of the existing variable stiffness solutions, the work has focused on beam-like elements, which stiffen by means of two different concepts: sliding segments and rotary movement.

It has to be noticed that a beam-element with variable stiffness can find use in several applications, such as flapping wings and fins, exoskeletons, prosthetics and endoscopes. Such elements could be designed as structures, manipulators, actuators or sensors. In latter case the controllable stiffness feature could be used to change the sensing sensitivity for stiff and soft applications.

The analysed components are characterized by a sort of discretized distributed variable stiffness: this in general can be interesting for continuous systems. For example, in wings and fins this distribution helps with the distributed interaction with the fluid, in endoscopes with the distributed interaction with the body.

Sliding segments solution worked well in case of a multi-material specimen: a significant bending stiffness variation has been shown. Its components were characterized by a strong stiffness difference between their alternated compli-

ant and rigid segments, emphasizing a multi-body interaction: the internal tube, when shifted, prevents outer tube's flexures to bend. This behaviour is found to depend linearly on the length of overlapped rigid parts, and to be independent from imposed displacement, for small displacements. Results have shown that changes in material properties work a lot better than changes in geometry.

In future works, this study can proceed in different aspects:

- Improvement of the experimental set-up: the use of a specific type of clamp, suitable for tubes, is suggested. Moreover, in case of a set-up with the same scheme of that described in section 5.2, it is really recommended to use an instrument with more resolution in measured force values, in order to get more precise results.
- A new analytical model could be implemented based on the achieved findings, such that the physical interaction between rod and tube as separate bodies would be relevant on the predicted results.
- Besides analytic modelling, numeric simulations with Finite Elements Method should be considered as a good option to study this concept. With a right pre-processing phase, enough computational power and well modelled interfaces between multiple bodies it should be possible to obtain reliable results.
- Future studies could also focus on the main limitations of this solution: about suitable materials, dimensions and possible types of actuation for an application inside a flapping wing.
- The flexure shifting principle could be implemented in future with two degrees of freedom, passing from beams to plates. By means of small displacements one could modify the flexural stiffness of the surface in one direction, or in the perpendicular one. In the Portwings project context, this approach could be applied to study variable stiffness wing surfaces between the more rigid spars.

- Up to now, flexures appear in rods and tubes with a constant spatial frequency, but different approaches can be tested. For instance, the ratio between the number of flexures present in the rod and the tube could be bigger than 1 (e.g. 1.5, 2, 3). In this way a lot of configurations can be generated, where only one or some flexure are aligned between the inner and the outer elements. By shifting the rod, the position of aligned flexures changes, allowing to achieve several different stiffness distributions with one single device 7.1.

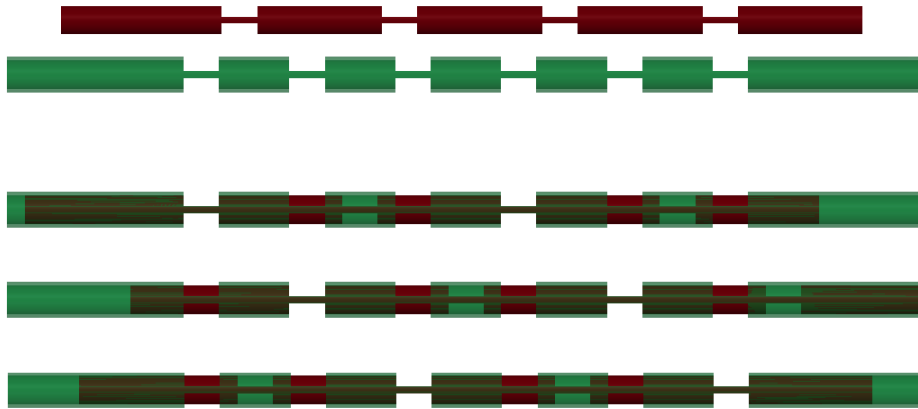


Figure 7.1: Example of alternative configurations achievable by changing flexures spatial frequency

The proposed rotary spar concept with multiple bending stiffness levels is also found to be working: it showed relevant stiffness variations and well distributed intermediate stiffness degrees between its limit values. Also in this case, stiffening is independent from the small imposed displacement.

The effects of deviated bending are successfully reduced by increasing beam flexural resistance in one direction, while keeping the inner part free to rotate. Furthermore, these positive results are obtained with a sample which was really problematic as a sliding segments solution.

The work can be carried on from multiple points of view:

- Optimization of geometrical parameters, in order to maximize the stiffness variation, while keeping load-bearing capabilities.
- This solution could be also integrated with variable stiffness sliding segments beams, allowing the internal rod both to translate and rotate (fig. 7.2). Possible advantages could be a bigger stiffness range and a bigger number of intermediate configurations, while possible disadvantages can include a more problematic actuation of the stiffening mechanism.
- In this work rotary spar and sliding segments solutions shared the same experimental set-up: also in this case, for future studies, more precise measurements are recommended.

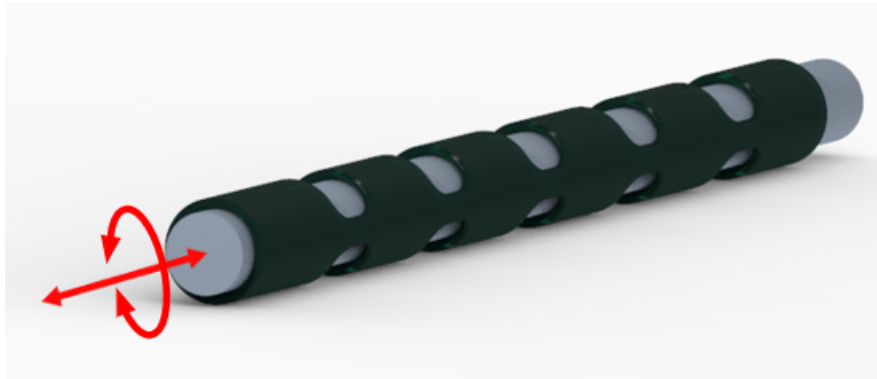


Figure 7.2: Possible integration of sliding segments and rotary spar



# Acknowledgements

I want to say thank you to all the people who helped me through these months: my relator prof. Parenti Castelli, who allowed me to take part to this wonderful experience; prof. Stramigioli, who involved me in this exciting project; my supervisor Alexander, who followed and guided me excellently throughout all the work; my friends Francesco and Federico, also involved in the Portwings project, who supported me and gave me useful ideas; my flatmates Ricardo, Giulia and Sarah; finally my friends Lorenzo, Marco and Federico, who managed to help me while being in three different countries. A special thanks also goes to my family, and all my other friends who made unique this experience in The Netherlands.



# Bibliography

- [1] G. A. Folkertsma, W. Straatman, N. Nijenhuis, C. H. Venner, S. Stramigioli, “Robird: a robotic bird of prey”, *IEEE Robotics & Automation Magazine*, 2017
- [2] “The PortWings Project”, [www.portwings.eu](http://www.portwings.eu)
- [3] L. Blanc, A. Delchambre, P. Lambert, “Flexible medical devices: review of controllable stiffness solutions”, *Actuators*, 2017
- [4] M. Manti, V. Cacucciolo, M. Cianchetti, “Stiffening in soft robotics”, *IEEE Robotics and Automation Magazine*, 2016
- [5] L. Wang *et al.*, “Controllable and reversible tuning of material rigidity for robot applications”, *Materials Today*, 2018
- [6] I. K. Kuder, A. F. Arrieta, W. E. Raither, P. Ermanni, “Variable stiffness material and structural concepts for morphing applications”, *Progress in Aerospace Sciences*, 2013
- [7] S. Mintchev, J. Shintake, D. Floreano, “Bioinspired dual-stiffness origami”, *Science Robotics*, 2018
- [8] M. B. Oliveira, C. Liu, M. Zhao, S. M. Felton, “Design of a variable stiffness wrist brace with an origami structural element”, *Science Robotics*, 2018
- [9] G. Brown, R. Haggard, B. Norton, “Inflatable structures for deployable wings”, *AAIA*, 2001

- [10] F. Dai, H. Li, S. Du, “A multi-stable lattice structure and its snap-through behavior among multiple states”, *Composite Structures*, 2012
- [11] W. Raither, M. Heymanns, A. Bergamini, P. Ermanni, “Morphing wing structure with controllable twist based on adaptive bending-twist coupling”, *Smart Materials and Structures*, 2013
- [12] W. Raither, L. De Simoni, L. Di Lillo, A. Bergamini, P. Ermanni, “Adaptive-twist airfoil based on electrostatic stiffness variation”, *AIAA/ASME/AHS Adaptive Structures Conference*, 2014
- [13] R. Vos, R. Breuker, R. Barrett, P. Tiso, “Morphing wing flight control via postbuckled precompressed piezoelectric actuators”, *Journal of Aircraft*, 2017
- [14] A. Cox, D. Monopoli, D. Cveticanin, M. Goldfarb, E. Garcia “The development of elastodynamic components for piezoelectrically actuated flapping Micro Air Vehicles”, *Journal of Intelligent Material Systems and Structures*, 2002
- [15] M. McEvoy, N. Correll, “Shape change through programmable stiffness”, *Experimental Robotics*, 2015
- [16] N. Cheng, A. Gopinath, L. Wang, K. Iagnemma, A. Hosoi, “Thermally tunable, self-healing composites for soft robotic applications”, *Macromolecular Materials and Engineering*, 2014
- [17] N. Cheng, G. Ishigami, S. Hawthorne, H. Chen, M. Hansen, M. Telleria, R. Playter, K. Ignanemma, “Design and analysis of a soft mobile robot composed of multiple thermally activated joints driven by a single actuator”, *IEEE International Conference on Robotics and Automation*, 2010
- [18] R. Poon, J. B. Hopkins, “Phase-changing metamaterial capable of variable stiffness and shape morphing”, *Advanced Engineering Materials*, 2019

- [19] A. Cox, K. Massey, E. Abdullah, “Wing morphing control via shape memory alloy actuators”, *Journal of Intelligent Material Systems and Structures*, 2013
- [20] Y. Dong, Z. Boming, L. Jun, “A changeable aerofoil actuated by shape memory alloy springs”, *Materials Science and Engineering: A*, p. 243-250, 2013
- [21] L. Hines, V. Arabagi, M. Sitti, “Shape memory polymer-based flexure stiffness control in a miniature flapping-wing robot”, *IEEE Transactions on Robotics*, 2012
- [22] S. Dastoor, M. Cutkosky, “Design of dielectric electroactive polymers for a compact and scalable variable stiffness device”, *IEEE International Conference on Robotics and Automation*, 2012
- [23] A. Sadeghi, L. Beccai, B. Mazzolai, “Innovative soft robots based on electro-rheological fluids”, *2012 IEEE/RSJ International Conference on Intelligent Robots and Systems*, 2012
- [24] J. Scheidler, V. Asnani, M. Dapino, “Dynamically tuned magnetostrictive spring with electrically controlled stiffness”, *Smart Materials and Structures*, 2016
- [25] K. Shanmuganathan, J. Capadona, S. Rowan, C. Weder, “Biomimetic mechanically adaptive nanocomposites”, *Progress in Polymer Science*, p. 212-222, 2010
- [26] J. R. Amend Jr. *et al.*, “A positive pressure universal gripper based on the jamming of granular material”, *IEEE Transactions on Robotics*, 2012
- [27] T. Wang, Y. Li, J. Zhang, J. Hong, M. Y. Wang, “A fluid-filled tubular dielectric elastomer variable stiffness structure by the hydrostatic skeleton principle”, *IEEE Transactions on Robotics*, 2013
- [28] Y. Kim, S. Cheng, S. Kim, K. Iagnemma, “A novel layer jamming mechanism with tunable stiffness capability for minimally invasive surgery”, *IEEE Transactions on Robotics*, 2013

- [29] T. Wang, J. Zhang, Y. Li, J. Hong, M. Y. Wang, “Electrostatic Layer Jamming variable stiffness for soft robotics”, *IEEE/ASME Transactions on Mechatronics*, 2019
- [30] A. J. Loeve, D. H. Plettenburg, P. Breedveld, J. Dankelman, “Endoscope shaft-rigidity control mechanism: “Forguide””, *IEEE Transactions on Biomedical Engineering*, 2012
- [31] Y. Kim, S. Cheng, S. Kim, K. Iagnemma, “A stiffness-adjustable hyperredundant manipulator using a variable neutral-line mechanism for minimally invasive surgery”, *IEEE Transactions on Robotics*, 2014
- [32] Y. Jiang, D. Chen, C. Liu, J. Li, “Chain-like granular jamming: a novel stiffness-programmable mechanism for soft robotics”, *Soft Robotics*, 2018
- [33] T. M. Huh, Y. Park, K. Cho, “Design and analysis of a stiffness adjustable structure using an endoskeleton”, *Soft Robotics*, 2018
- [34] M. Jiang, “Sliding layer laminates: a new robotic material enabling robust and adaptable undulatory locomotion”, *UC San Diego Electronic Theses and Dissertations*, <https://escholarship.org/uc/item/1818q867#main>, 2018
- [35] Y. Park *et al.*, “Dual-stiffness structures with reconfiguring mechanism: design and investigation”, *Journal of Intelligent Material Systems and Structures*, 2015
- [36] A. Stilli *et al.*, “A novel concept for safe, stiffness-controllable robot links”, *Soft Robotics*, 2017
- [37] R. Tiwari, M. A. Meller, K. B. Wajcs, C. Moses, I. Reveles, E. Garcia, “Hydraulic artificial muscles”, *Journal of Intelligent Material Systems and Structures*, 2012
- [38] M. Philen, Y. Shan, K. W. Wang, C. E. Bakis, C. D. Rahn, “Fluidic flexible matrix composites for the tailoring of variable stiffness adaptive structures”, *AIAA/ASME/ASCE/AHS/ASC Structures, Structural Dynamics, and Materials Conference*, 2007

- [39] S. S. Groothuis, G. Rusticelli, A. Zucchelli, S. Stramigioli, R. Carloni, “The vsaUT-II: a novel rotational variable stiffness actuator”, *IEEE International Conference on Robotics and Automation*, 2012
- [40] M. Amprikidis, J. E. Cooper, “Development of smart spars for active aeroelastic structures”, *AIAA/ASME/ASCE/AHS Structures, Structural Dynamics, and Materials Conference*, 2003
- [41] B.Vanderborgh *et al.*, “Variable impedance actuators: a review”, *Robotics and Autonomous Systems*, 2013
- [42] L. Xu *et al.*, “Artificial muscle with reversible and controllable deformation based on stiffness-variable carbon nanotube spring-like nanocomposite yarn”, *The Royal Society of Chemistry*, 2019
- [43] D. C. F. Li, Z. Wang, B. Ouyang, Y. H. Liu, “A reconfigurable stiffness manipulator by a sliding layer mechanism”, *International Conference on Robotics and Automation (ICRA)*, 2019
- [44] H. Soemers, “Design principles for precision mechanisms”, *T-Point Print VoF*, 2010
- [45] “PolyJet 3D Printing Technologies Simply Explained”, <https://all3dp.com>
- [46] “SMAC Moving Coil Actuators”, [www.smac-mca.com](http://www.smac-mca.com)